2004

Stress field variations in the Swiss Alps and the northern Alpine foreland derived from inversion of fault plane solutions

Ulrike Kastrup
Insitute of Geophysics

Mary Lou Zoback
U.S. Geological Survey, marylouz@stanford.edu

Nicholas Deichmann
Insitute of Geophysics

Keith Evans
Geology Institute

Domenico Giardini
Insitute of Geophysics

See next page for additional authors

Stress field variations in the Swiss Alps and the northern Alpine foreland derived from inversion of fault plane solutions

Ulrike Kastrup,[1] Mary Lou Zoback,[2] Nicholas Deichmann,[1] Keith F. Evans[1,3] Domenico Giardini,[1] and Andrew J. Michael[2]

Received 22 April 2003; revised 13 July 2003; accepted 19 August 2003; published 3 January 2004.

[1] This study is devoted to a systematic analysis of the state of stress of the central European Alps and northern Alpine foreland in Switzerland based on focal mechanisms of 138 earthquakes with magnitudes between 1 and 5. The most robust feature of the results is that the azimuth of the minimum compressive stress, S_3, is generally well constrained for all data subsets and always lies in the NE quadrant. However, within this quadrant, the orientation of S_3 changes systematically both along the structural strike of the Alpine chain and across it. The variation in stress along the mountain belt from NE to SW involves a progressive, counterclockwise rotation of S_3 and is most clear in the foreland, where it amounts to 45°–50°. This pattern of rotation is compatible with the disturbance to the stress field expected from the indentation of the Adriatic Block into the central European Plate, possibly together with buoyancy forces arising from the strongly arcuate structure of the Moho to the immediate west of our study area. Across the Alps, the variation in azimuth of S_3 is defined by a progressive, counterclockwise rotation of about 45° from the foreland in the north across the Helvetic domain to the Penninic nappes in the south and is accompanied by a change from a slight predominance of strike-slip mechanisms in the foreland to a strong predominance of normal faulting in the high parts of the Alps. The observed rotation can be explained by the perturbation of the large-scale regional stress by a local uniaxial deviatoric tension with a magnitude similar to that of the regional differential stress and with an orientation perpendicular to the strike of the Alpine belt. The tensile nature and orientation of this stress is consistent with the "spreading" stress expected from lateral density changes due to a crustal root beneath the Alps. *INDEX TERMS:* 7230 Seismology: Seismicity and seismotectonics; 8122 Tectonophysics: Dynamics, gravity and tectonics; 8164 Tectonophysics: Stresses—crust and lithosphere; *KEYWORDS:* earthquake, focal mechanism, stress rotation, stress inversion, Swiss Alps, gravitational potential energy

Citation: Kastrup, U., M. L. Zoback, N. Deichmann, K. F. Evans, D. Giardini, and A. J. Michael (2004), Stress field variations in the Swiss Alps and the northern Alpine foreland derived from inversion of fault plane solutions, *J. Geophys. Res.*, *109*, B01402, doi:10.1029/2003JB002550.

1. Introduction

[2] The Alps are the most prominent young tectonic structure in Europe: they represent the western European segment of the Tertiary collision zone between the African and the Eurasian continents (Figure 1a). Present convergence rates of up to 9 mm/yr have been estimated for the relative motion between Africa and Europe [*DeMets et al.*, 1994]. In this study we address the question of whether compression related to the collision is still the dominant force acting in the Alps and Alpine foreland or whether the present stress field reflects local perturbations due to other causes. Answers to this question are not only of interest for our understanding of the tectonic processes and evolution of the Alps but are also pertinent to the problem of seismic source zonation for earthquake hazard assessment.

[3] Earthquake focal mechanisms are among the most valuable sources of information for assessing the state of stress of the Earth's crust. *Pavoni* [1975, 1977] used the direction of the deformational axes, *P* (compression) and *T* (extension), obtained from fault plane solutions in a first attempt to estimate the state of stress in Switzerland. His results indicate a fan-like spreading of the compressional axes perpendicular to the mountain belt. Since these early studies, the number and quality of available focal mechanisms has increased steadily and new methods of in situ stress measurement have been implemented. The data available until about 1990 have been compiled in the World Stress Map project to produce a map of stress directions and relative magnitudes for western Europe [*Müller et al.*, 1992, 1997; *Zoback*, 1992]. On a regional scale these studies largely confirm *Pavoni*'s [1975, 1977] observation of a fan-like rotation of horizontal stresses north of the Alpine front

[1]Institute of Geophysics, ETH-Hönggerberg, Zürich, Switzerland.
[2]Western Region Earthquake Hazard Team, U.S. Geological Survey, Menlo Park, California, USA.
[3]Now at Geology Institute, ETH-Hönggerberg, Zürich, Switzerland.

0148-0227/04/2003JB002550$09.00

that can be related to the ongoing convergence of Africa and Europe. However, recent more detailed studies suggest that there exist significant local deviations from this regional stress field.

[4] In the Jura Mountains and the northern part of the Molasse Basin, numerous in situ stress measurements have been carried out at depths of a few meters [e.g., *Greiner and Illies*, 1977; *Becker et al.*, 1987; *Becker*, 1999], and stress-induced borehole breakouts have been observed in deep wells [*Blümling et al.*, 1992]. Analyses of the orientation of *P* and *T* axes as well as stress inversions have been performed on earthquake fault plane solutions for several areas, which include the southern Rhine Graben, parts of northern Switzerland, the Wallis, the western Alps, and the

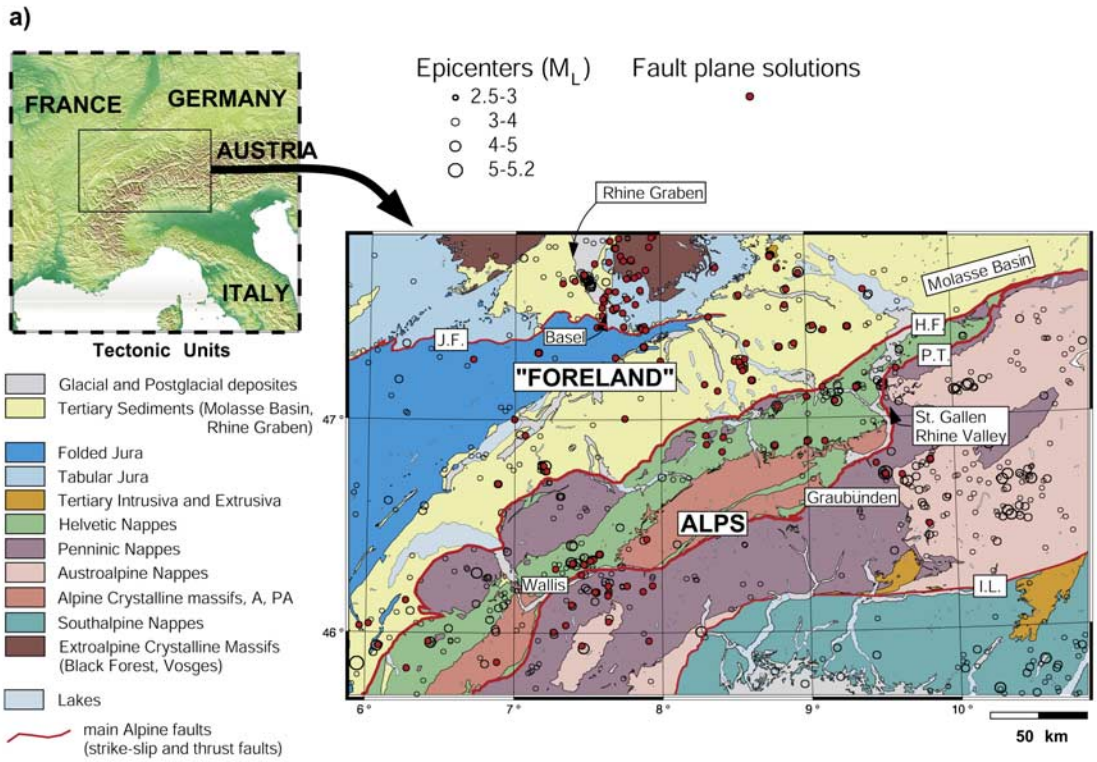

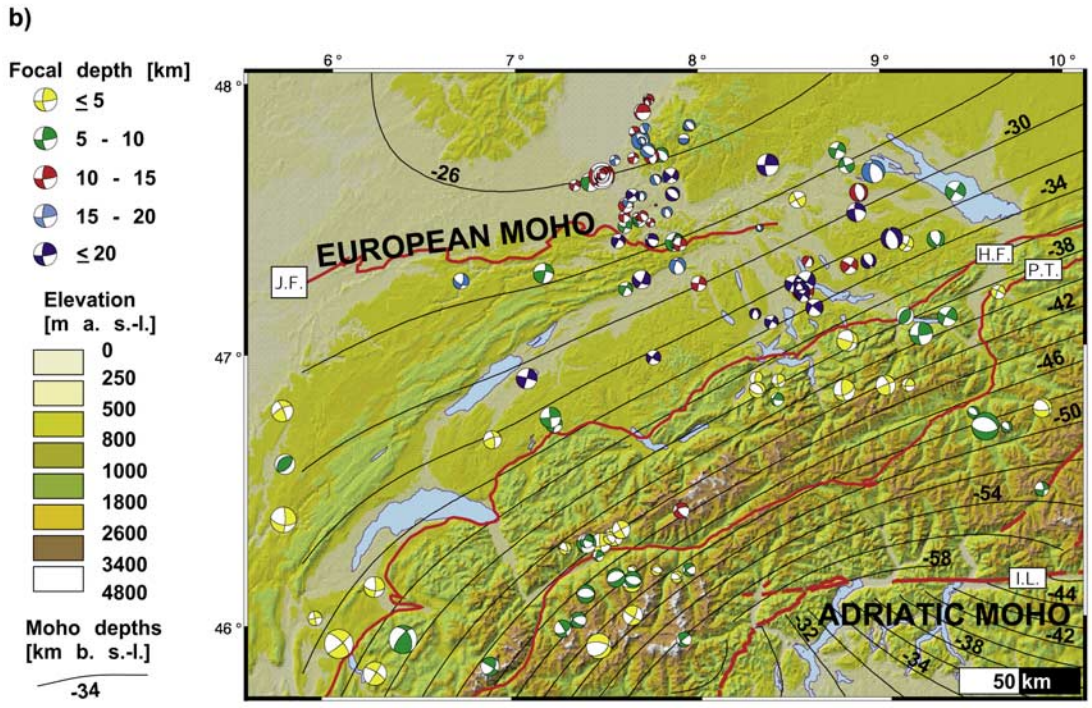

western part of the Po Plain [*Roth et al.*, 1992; *Plenefisch and Bonjer*, 1997; *Maurer et al.*, 1997; *Eva et al.*, 1997; *Eva and Solarino*, 1998; *Evans and Roth*, 1998; *Sue et al.*, 1999; *Deichmann et al.*, 2000b]. To date, however, no comprehensive stress analysis has been performed for the whole northern Alpine foreland and central Alps. This is the objective of the present paper. We have compiled a data set of 138 high-quality earthquake focal mechnisms and applied *Gephart and Forsyth*'s [1984] as well as *Michael*'s [1984] stress inversion methods to different subsets of these data to investigate spatial variations in stress orientation and relative magnitudes. As there is some controversy regarding the reliability of the uncertainty estimates of the different inversion methods [e.g., *Hardebeck and Hauksson*, 2001], the comparison of the results of the two methods allows us to assess the significance of possible spatial stress variations with more confidence. Our results confirm earlier observations of a fan-like rotation of the axis of maximum compression in the northern foreland. In addition, they present evidence for a systematic rotation of the least compressive stress and for a change in style of faulting between the foreland and the highest parts of the Alps in Switzerland. We interpret this in terms of the superposition of a local uniaxial tensional stress, related to spreading effects within the orogen, upon the regional compressive stress, associated with the large-scale continental convergence.

2. Tectonic Setting

[5] The European Alps are the most significant young tectonic structure in central Europe. They stretch in an arc around northern Italy, striking more or less N-S in the west and bending to an ENE-WSW strike at the latitude of Switzerland (Figure 1a). Throughout this paper we refer to the westernmost portion of the Alps between France and Italy as the western Alps, the easternmost part in Austria as the eastern Alps, and the Swiss part in between as the central Alps. (Note that 'western' and 'eastern' are adjectives (hence the first letter is lower case), and that the ''western Alps' must not be confused with the 'Western Alps' mountain range which comprises our western Alps as well as the Alps in western Switzerland (Wallis). Similarly, the conventional 'Eastern Alps' include the Alps in eastern Switzerland and beyond. There is no Central Alps mountain range.) The tectonics of Switzerland are deeply influenced by the Alpine orogeny because the country lies within the Tertiary collision zone between the African and the Eurasian plates. N-S convergence between the African and the Eurasian plates began approximately 120 Myr ago and was related to a counterclockwise rotation of the African plate. After the Alpine Tethys ocean, which lay in between Eurasia and the African microplate Adria, had been subducted to the south, the two continents collided in the area of the eastern Alps at about 65 Ma. [e.g., *Schmid et al.*, 1996, 1997]. As convergence continued, the upper crustal parts of the Adriatic continental microplate were thrust over the oceanic and European crust while the lower Adriatic crust and upper mantle intruded into Eurasia, splitting the Eurasian crust horizontally [*Pfiffner et al.*, 1997]. During the early Miocene (about 23 Ma), the continuing indentation of the Adriatic plate caused the uplift of the Alps, while the debris of the rising mountains were deposited in the foreland basin to the north to form the Molasse Basin. Continuous crustal shortening resulted in the most recent tectonic movements north of the Alps which affected the foreland basin. This deformation started less than 12 Myr with the overthrust of the most southern parts of the Molasse (Subalpine Molasse) and produced a slight folding of the entire Molasse section. Finally, detachment along Triassic evaporites in northwestern Switzerland and eastern France and continued compressional deformation formed the Jura Mountains around 3–5 Ma. Whether the foreland is still active as a fold and thrust belt [e.g., *Meyer et al.*, 1994; *Calais*, 1999] or whether this deformation has ceased or changed is subject to debate [e.g., *Becker*, 1999].

[6] The major tectonic units in the area of Switzerland are shown in Figure 1a. They are the Molasse Basin, the Jura Mountains and the Alps proper. A further subdivision can be made within the Alps by distinguishing between members of the series of stacked nappes. Generally, the higher the relative position of a nappe, the further south its origin. The three major nappes from top to bottom are the Eastern Alpine nappes which originated from the Adriatic plate, the Penninic nappes, which were located in the region of the Alpine Tethys, and the Helvetic nappes which derive from the margin of the Eurasian continent [see *Schmid and Kissling*, 2000, Figure 1]. The Penninic nappes are separated from the Helvetic nappes by the Basal Penninic Thrust. Further north, the Helvetic nappes are separated from the foreland by the Helvetic front.

3. Seismicity and Focal Mechanism Data

[7] Seismicity in Switzerland has been monitored since the mid 1970s by a dense short period telemetered network operated by the Swiss Seismological Service [*Baer*, 1990].

Figure 1. (a) Seismicity (1975–1999; $M_L > 2.5$), fault plane solutions (1961–1999), and principal tectonic units in Switzerland. PA, para-autochthonous; A, autochthonous; J.F., Jura front; H.F., Helvetic front, P.T., Penninic thrust; I.L., Insubric Line. The Helvetic nappes lie between the Helvetic front and the Penninic thrust with the foreland to the north and the Penninic nappes to the south. The Helvetic and Penninic nappes constitute the Alps proper, the Swiss part of which is denoted in this paper as the central Alps. The French/Italian parts are referred to as the ''western Alps'' and the Austrian part is referred to as the ''eastern Alps'' (not to be confused with the conventional western Alps and eastern Alps which extend into Switzerland). The tectonic map is a simplified version of the Digital Tectonic Map of Switzerland of the Swiss Federal Office of Water and Geology. (b) Location, focal mechanisms, and depth of events used in the study superimposed on topographic map. The contours denote the depth to the Moho. H.F., Helvetic front; P.T., Penninic thrust; I.L., Insubric Line. The surface topography is from the digital elevation model ''RIMINI'' and is reproduced with the permission from the Swiss Federal Office of Topography. It is complemented with data from the 30" elevation model (GTOPO30) of the U.S. Geological Survey.

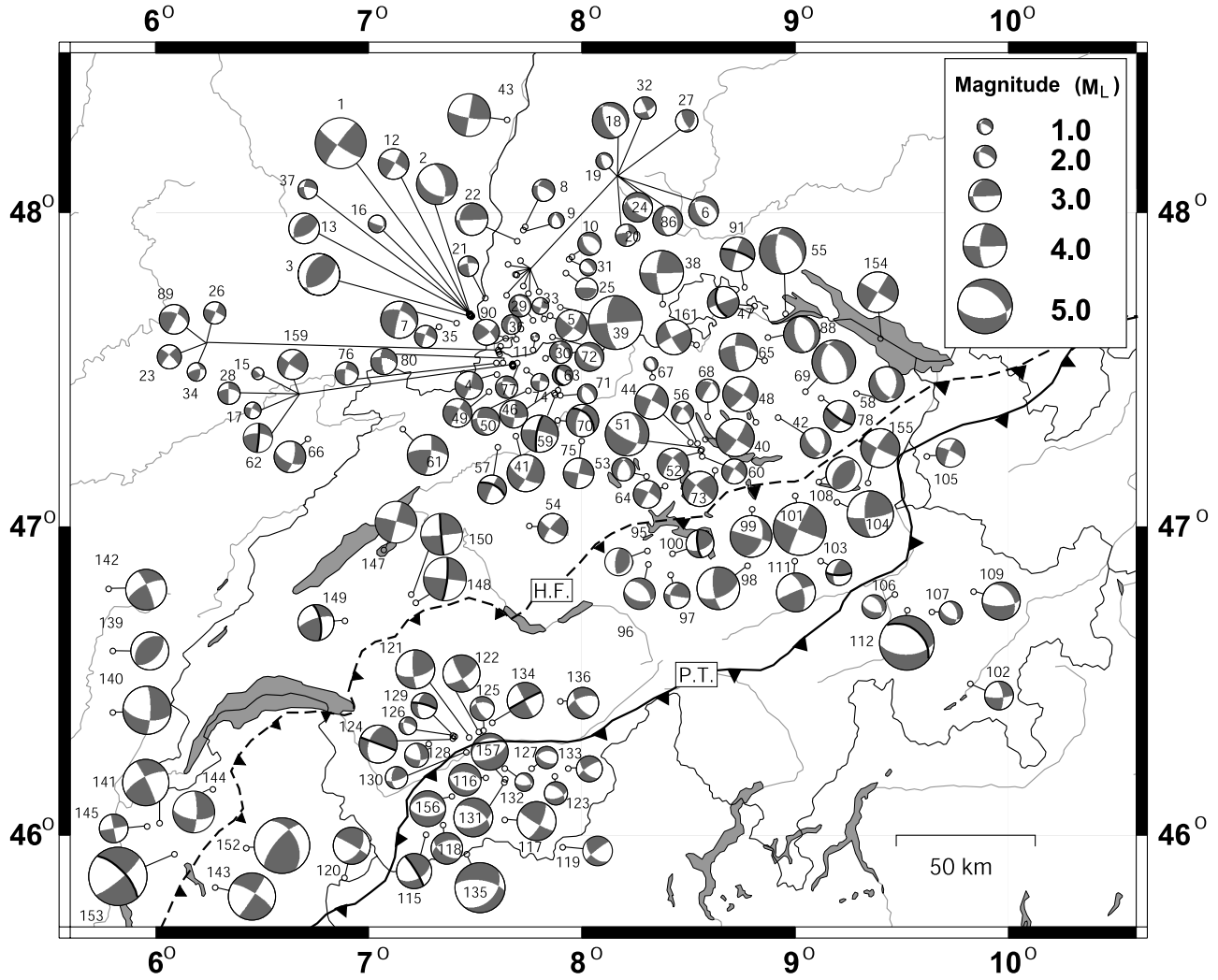

Figure 2. Lower hemisphere, equal-area projection for the 138 fault plane solutions in Switzerland and adjacent areas which are used in this study (1961–1998). The active fault plane is known for 20 of the events from aftershock studies and is distinguished by the thick black line. The numbers refer to the FPS index number in Table 1.

All waveforms have been available in digital form since the end of 1983. The permanent national network has been augmented from time to time by several temporary local networks [*Roth*, 1990; *Maurer*, 1993; *Baer*, 1990]. Stations in neighboring countries are also utilized for constraining the location and the fault plane solutions of earthquakes situated on the periphery or outside the Swiss network (see acknowledgments for list of institutions that supplied data for this study).

[8] The collision between the African and the Eurasian Plate is currently most active in southeastern Europe along the Adriatic and the Mediterranean Sea. In comparison, in Switzerland, where the Tertiary collision zone was located, seismicity is only low to moderate. Relatively high levels of seismicity are found in the southern Rhine Graben area, the Rhine Valley of St. Gallen, in Graubünden, and in the Wallis (Figure 1a).

[9] Earthquake hypocenters within the Alps proper are restricted to the upper ~15 km of the crust, while earthquakes in the northern foreland occur throughout the crust down to the Moho found at ~30 km [*Deichmann and Rybach*, 1989; *Deichmann and Baer*, 1990; *Deichmann*, 1992; *Deichmann et al.*, 2000a, 2000b] (Figure 1b).

[10] The fault plane solutions of 138 earthquakes recorded between 1961 and 1998, with magnitudes of between M_L = 1.1 and 5.2, have been compiled for the present study (Figures 1b and 2 and listed in Table 1). FPSs with a magnitude of less than $M_L \leq 2.0$ in northern Switzerland and in the Wallis are based on data recorded by local temporary networks [*Maurer*, 1993; *Bonjer*, 1997; *Deichmann et al.*, 2000b]. As a consequence, despite their small magnitude, these FPSs are well constrained. The question remains whether focal mechanisms of such small events are representative of the regional stress field. In fact, focal mechanisms of small aftershocks often exhibit a large scatter due to stress perturbations caused by the main shock. However, the small earthquakes included in our study are mostly independent events and the fact that their focal mechanisms do not increase the scatter of observed *P* and *T* axis orientations confirms that these mechanisms can be regarded as representative and provide robust estimates of the stress field. New fault plane solutions as well as those

Table 1. List of All Events in Switzerland and Adjacent Areas for Which Fault Plane Solutions (FPS) Have Been Determined

							First Nodal Plane			Second Nodal Plane			*P* Axis		*T* Axis			
FPS	Date	Time	Lat	Lon	z	M_L	Strike	Dip	Rake	Strike	Dip	Rake	Strike	Dip	Strike	Dip	Location	Ref[a]
Foreland (Molasse Basin, Jura Mountains, Vosges, Black Forest) (West-1 to East-5)																		
F1																		
139	1968.02.05	0228	46.6	5.8	6	3.5	224	38	90	44	52	90	134	7	314	83	Clairvaux	3, 12, 4
140	1971.06.21	0725	46.4	5.8	3	4.4	99	57	−166	1	78	−34	315	32	54	14	Jeurre	3, 12, 4
141	1975.05.29	0032	46.04	6.02	0	4.2	242	70	174	334	84	20	106	10	200	18	Vuache[b]	5
144	1982.11.08	1302	46.15	6.27	4	3.8	97	62	−167	1	79	−29	316	28	52	12	Annemasse[b]	12
145	1983.11.16	0027	46.03	5.96	4	2.6	349	90	0	79	90	−180	304	0	34	0	Vuache	12[c]
153[d]	1996.07.15	0013	45.94	6.09	2	5.3	316[d]	70[d]	−11[d]	50	80	−160	274	22	181	7	Annecy	23
F2																		
146	1976.03.22	1444	47	7	0	2.7	13	90	0	283	90	180	148	0	58	0	St.Blaise	9, 4
147	1979.07.03	2113	46.93	7.07	30	3.8	285	86	179	15	89	4	150	2	240	4	Murten[b]	8, 9
148[d]	1987.09.20	1153	46.76	7.22	7	3.9	7[d]	81[d]	0[d]	277	90	171	323	6	232	6	Fribourg	28
61	1987.12.11	0225	47.31	7.16	79	3.7	274	70	168	8	79	20	140	6	232	22	Glovelier	14
149[d]	1988.10.14	1902	46.7	6.89	2	3.3	350[d]	69[d]	20[d]	253	71	158	302	2	211	29	Romont	28
66	1989.04.30	0338	47.28	6.72	19	2.9	115	61	−156	13	69	−31	332	36	66	5	Belleherbe	14
150[d]	1995.09.17	1629	46.78	7.2	7	3.8	175[d]	88[d]	3[d]	85	87	178	310	1	40	4	Fribourg	28
F3																		
4	1982.03.25	1845	47.49	7.6	7	2.5	110	79	−172	18	82	−11	334	13	64	2	Reinach	16
15	1987.12.31	1516	47.52	7.68	12	1.1	53	40	14	312	81	129	13	26	258	41	Pratteln	16
17	1988.05.11	1112	47.52	7.68	10	1.5	199	75	−16	293	75	−164	156	22	66	0	Pratteln	16
23	1989.05.05	1744	47.56	7.61	10	2.2	312	79	−170	220	80	−11	176	15	266	1	Basel	16
26	1990.06.16	2241	47.58	7.62	18	2	293	80	177	24	87	10	158	5	249	9	Weil	16
28	1990.07.25	1438	47.52	7.67	10	2	180	86	−32	272	58	−176	131	25	231	19	Pratteln	16
30	1990.11.28	0138	47.54	7.83	18	2	319	48	−130	190	55	−55	159	61	256	4	Möhlin	16
46	1982.09.03	1912	47.42	7.9	11	2.5	97	70	−175	5	85	−20	319	18	53	10	Hauenstein	8, 9
49	1984.04.10	1650	47.43	7.57	22	2.6	300	62	−176	208	87	−28	160	22	257	17	Breitenbach[b]	10
50	1984.04.12	0050	47.44	7.75	21	2.5	162	42	−30	275	71	−128	143	49	32	17	Bubendorf	10
54	1985.07.07	0008	47	7.75	30	2.7	124	80	169	216	79	10	170	1	80	15	Langnau i.E.[b]	10
57[d]	1987.01.08	1924	47.26	7.61	6	2.6	298[d]	62[d]	−174[d]	205	85	−28	158	23	255	16	Günsberg	14
59[d]	1987.04.11	0314	47.43	7.87	7	3.4	190[d]	76[d]	−11[d]	282	79	−166	146	18	56	2	Läufelfingen	14
62[d]	1987.12.16	0936	47.52	7.68	9	2.7	6[d]	86[d]	36[d]	273	54	175	134	21	236	28	Pratteln	14
63[d]	1988.04.16	1405	47.44	7.89	9	1.9	310[d]	63[d]	−108[d]	165	32	−59	187	67	53	16	Zeglingen	14
70	1996.12.15	0449	47.34	7.89	20	3	313	50	141	195	61	−47	158	53	256	6	Olten	18
71[d]	1997.02.21	0504	47.42	7.88	8	1.8	316[d]	55[d]	−114[d]	174	42	−60	171	69	63	7	Läufelfingen[b]	21
72	1997.09.02	0030	47.61	7.86	23	2.6	128	53	−90	308	37	−90	38	82	218	8	Möhlin	21
74	1988.10.27	2052	47.5	7.74	12	1.6	275	77	−177	184	87	−13	139	11	230	7	Liestal	27
75	1990.08.11	0531	47.27	8	15	2.8	11	90	0	281	90	180	326	0	236	0	Zofingen	27
76	1990.08.16	1839	47.52	7.6	11	2.1	282	61	−167	186	79	−30	140	29	237	12	Reinach	27
77	1990.11.08	1938	47.52	7.7	11	2	282	50	−141	164	61	−47	127	53	225	6	Pratteln	27
89	1996.04.24	0936	47.57	7.61	12	2.7	292	55	174	25	85	35	153	20	254	28	Basel	27
11	1986.11.01	0401	47.57	7.77	19	1.2	296	81	−174	205	84	−9	160	11	251	2	Dinkelberg	16
36	1991.11.05	0913	47.6	7.69	17	1.8	334	43	−122	194	55	−64	160	68	266	7	Lörrach	16
41	1978.08.13	0402	47.29	7.69	24	3.4	121	66	−168	26	79	−24	341	25	75	8	Önsingen	8, 9
80	1992.03.25	0533	47.52	7.63	8	2.6	278	65	−160	179	72	−26	137	31	230	5	Muttenz	27
90	1996.06.15	0105	47.6	7.64	21	2.4	314	73	165	48	76	17	180	2	271	23	Basel	27
159	1999.07.13	2047	47.51	7.7	19	2.7	215	70	−5	307	85	−160	173	17	79	11	Pratteln	26
F4																		
1	1980.07.15	1217	47.67	7.48	12	4.7	125	80	174	216	84	10	350	3	81	11	Sierentz	29,16
2	1980.07.15	1254	47.67	7.49	10	3.7	117	46	−132	349	58	−55	314	60	55	6	Sierentz	16
3	1980.07.16	1500	47.67	7.48	13	3.8	201	42	64	54	53	111	129	6	21	72	Sierentz	16
5	1982.10.04	0406	47.67	7.85	23	2.9	36	74	−6	128	84	−164	353	15	261	7	Wiesental	16
6	1984.06.16	0643	47.75	7.8	9	2.7	295	41	−118	150	55	−68	113	70	225	8	Wies	16
7	1985.02.28	2133	47.65	7.41	10	3.4	292	49	−169	195	82	−41	145	34	250	21	Sierentz	16
8	1985.09.15	1818	47.95	7.73	14	2	180	44	−33	295	68	−129	160	51	52	14	Munzingen	16
9	1986.01.20	0348	47.95	7.73	12	1.4	200	40	−48	330	61	−119	193	62	81	12	Bad Krotzingen	16
10	1986.10.07	2223	47.86	7.95	18	2.1	297	42	−114	148	52	−70	116	74	224	5	Todtnau	16
12	1987.07.18	0859	47.67	7.48	12	2.8	299	80	177	30	87	10	164	5	255	9	Sierentz	16
13	1987.11.21	1401	47.68	7.48	12	2.8	209	38	64	61	56	109	138	9	18	72	Sierentz	16
16	1988.03.23	2111	47.68	7.47	11	1.6	7	30	−13	108	84	−119	350	44	222	33	Sierentz	16
18	1988.08.26	0030	47.8	7.69	19	3.3	307	30	−118	158	64	−75	97	67	237	18	Badenweiler	16
19	1988.08.28	2045	47.8	7.69	20	1.5	296	33	−134	165	67	−66	111	61	237	19	Badenweiler	16
20	1988.10.18	1119	47.74	7.65	12	2	272	73	170	5	80	17	138	5	229	19	Feuerbach	16
21	1988.11.20	2043	47.73	7.55	17	1.9	263	68	−177	172	87	−22	125	17	220	13	Bad Bellingen	16
22	1989.03.18	1426	47.91	7.7	14	3	184	27	7	88	87	117	154	36	23	42	Bad Krotzingen	16
24	1989.08.12	1419	47.77	7.73	19	2.7	275	35	−120	130	60	−71	80	69	206	13	Marzell	16
25	1990.05.11	0629	47.81	7.92	20	2	58	14	56	273	78	98	356	33	193	56	Utzenfeld	16
27	1990.06.20	1059	47.85	7.71	17	2	31	35	145	151	71	60	263	20	24	54	Sulzburg	16

Table 1. (continued)

							First Nodal Plane			Second Nodal Plane			*P* Axis		*T* Axis			
FPS	Date	Time	Lat	Lon	*z*	M_L	Strike	Dip	Rake	Strike	Dip	Rake	Strike	Dip	Strike	Dip	Location	Ref[a]
29	1990.07.31	1913	47.66	7.77	19	2	318	21	−109	158	70	−83	80	64	243	25	Steinen	16
31	1990.12.11	0910	47.85	7.94	13	1.5	92	35	−132	320	65	−65	269	62	32	16	Todtnauberg	16
32	1991.01.01	0729	47.84	7.65	12	2	68	63	−176	336	87	−27	288	21	25	16	Laufen	16
33	1991.05.20	0013	47.66	7.82	17	1.5	105	73	−170	12	80	−17	328	19	59	5	Hausern	16
34	1991.06.04	1717	47.55	7.61	7	1.7	360	56	24	256	70	144	311	9	213	39	Basel	16
35	1991.08.25	0006	47.64	7.33	12	2	292	76	−172	200	82	−14	155	16	247	4	Mulhouse	16
37	1991.11.12	1910	47.68	7.48	12	1.8	175	59	−22	277	71	−147	139	36	44	8	Sierentz	16
43	1979.10.27	1458	48.29	7.65	7	3.9	100	80	180	190	90	10	325	7	55	7	Rhinau[b]	7
86	1995.01.10	1126	47.74	7.75	14	2.7	336	36	−108	178	56	−77	126	75	259	10	Dinkelberg	29
39	1961.04.28	2048	47.7	7.9	0	4.9	176	64	0	86	90	154	134	18	38	18	Zell	2, 9
										F5								
38	1992.12.30	2134	47.71	8.38	22	4	181	71	3	90	87	161	137	11	44	15	Wutöschingen	20, 26
67	1989.06.09	0130	47.48	8.33	18	1.3	142	42	−105	342	50	−77	311	79	63	4	Wettingen[b]	14
161	1999.09.12	1325	47.58	8.54	2	3.1	151	80	175	242	85	10	16	3	107	11	Eglisau	26
47[d]	1983.09.04	2151	47.7	8.81	8	2.8	159[d]	74[d]	175[d]	250	85	16	24	8	116	15	Diessenhofen	13
55	1986.02.27	1207	47.68	8.96	17	4.2	304	38	−138	179	65	−60	131	58	247	15	Steckborn	10
65	1989.02.21	2336	47.53	8.86	22	3.5	273	62	−165	176	77	−29	131	30	227	10	Islikon[b]	14
88	1995.06.25	1853	47.6	8.87	12	3.3	167	58	−90	347	32	−90	77	77	257	13	Frauenfeld	27
91[d]	1996.06.28	0343	47.76	8.76	9	3.1	289[d]	78[d]	−172[d]	197	82	−12	153	14	244	3	Singen	27
154	1976.03.02	0827	47.6	9.4	10	3.7	31	90	0	301	90	180	346	0	76	0	Bodensee	9
42	1978.08.28	1444	47.35	8.92	22	2.8	9	40	−46	137	62	−120	1	60	249	12	Baeretswil	7, 11, 9
48	1984.01.11	1411	47.34	8.82	11	3.2	36	76	5	304	85	166	351	6	259	13	Wetzikon	10, 11, 9
58	1987.01.29	0007	47.43	9.29	8	3.2	10	45	−54	144	55	−121	357	65	255	6	Herisau[b]	14
69	1996.08.24	0238	47.43	9.05	29	4	184	42	−63	330	53	−112	183	72	75	6	Kirchberg	18
78[d]	1990.01.05	0421	47.41	9.12	5	2.9	126[d]	78[d]	−160[d]	32	70	−13	350	23	258	5	Lütisburg	27
40	1977.11.21	1927	47.28	8.58	25	3.5	33	80	−5	124	85	−170	349	11	258	4	Horgen[b]	8, 11, 9
44	1979.11.30	0044	47.27	8.51	27	3.1	296	84	−176	206	86	−6	161	7	251	1	Albis	8, 11, 9
51	1984.09.05	0516	47.25	8.56	15	4	8	44	−26	117	72	−131	345	46	236	17	Albis	10, 11, 9
52	1984.09.14	2230	47.24	8.56	24	2.9	315	67	−158	216	70	−25	175	31	266	2	Albis	10
53	1985.01.07	0952	47.16	8.3	27	2.1	336	46	−125	201	54	−59	170	65	270	4	Hochdorf	10
56	1986.10.08	0312	47.27	8.54	28	2	315	66	−160	217	72	−25	174	30	267	4	Albis	10
60	1987.05.05	2029	47.23	8.56	29	2.3	304	75	−170	211	80	−15	167	18	258	4	Albis	14
64	1988.09.11	2301	47.13	8.39	29	2.5	298	74	180	28	90	16	162	11	254	11	Root	14
68	1989.10.24	1203	47.35	8.59	12	2.1	314	30	−166	212	83	−61	150	44	278	32	Zürich	14
73	1997.10.23	1207	47.18	8.62	30	3.2	221	65	−2	312	88	−155	179	19	84	16	Menzingen	21
										Helvetic Nappes (West-1 to East-3)								
										H1								
143	1980.12.02	0558	45.83	6.28	1	4.3	302	76	−4	33	86	−166	258	13	167	7	Annecy	6
152	1994.12.14	0856	45.96	6.43	10	4.5	332	44	29	220	70	130	282	15	173	49	Grand Bornand	19
										H2								
121	1986.10.09	1008	46.32	7.47	4	3.6	79	61	167	175	79	30	304	12	41	28	Zeuzier	19
122	1989.01.07	0229	46.34	7.54	4	3.4	57	68	170	151	81	22	282	9	16	22	Montana	19
124[d]	1989.09.30	0441	46.32	7.39	6	3.5	110[d]	90[d]	140[d]	200	50	0	163	27	57	27	Anzere	17
125	1990.04.28	2224	46.34	7.52	3	2.2	266	46	−145	150	65	−50	108	52	212	11	Montana	17
126	1990.05.07	1606	46.32	7.4	7	1.6	175	45	−31	288	69	−131	153	49	46	14	Anzere	17
128	1990.06.03	1923	46.3	7.28	3	2.2	100	60	−151	354	65	−34	315	41	48	3	Sanetsch	17
129[d]	1990.07.26	1230	46.33	7.4	7	2.4	285[d]	80[d]	−140[d]	187	51	−13	154	35	50	19	Anzere	17
130	1990.08.31	1057	46.27	7.46	7	2	181	53	25	75	70	140	132	11	32	42	St. Leonard	17
134[d]	1996.02.21	1857	46.37	7.58	5	3.3	242[d]	87[d]	−178[d]	152	88	−3	107	4	197	1	Leukerbad	24
136	1997.11.28	0830	46.44	7.9	12	2.9	250	60	−150	144	64	−34	105	41	198	3	Lötschental	21
										H3								
94	1964.03.14	2044	46.9	8.3	0	5.2	189	51	27	81	69	138	139	11	37	44	Sarnen	1, 9, 27
95	1985.09.29	2336	46.92	8.31	1	2.5	39	26	122	184	68	75	285	22	70	64	Kerns	27
96	1985.12.21	1719	46.88	8.31	2	2.9	320	46	−63	104	50	−115	307	71	211	2	Sachseln	27
97	1989.11.19	2120	46.85	8.42	6	2.4	196	45	8	100	84	135	157	25	47	35	Engelberg	27
98	1994.08.28	0604	46.88	8.78	4	3.9	68	56	156	172	70	36	297	9	34	39	Schaechental	27
99	1995.11.16	0557	47.06	8.8	4	3.8	16	45	0	286	90	135	341	30	231	30	Iberg	27
100[d]	1996.12.07	0534	46.91	8.43	2	2.5	172[d]	74[d]	36[d]	70	56	160	297	11	36	37	Oberrickenbach	27
101	1971.09.29	0719	47.1	9	0	4.8	113	86	176	203	86	4	158	0	68	6	Naefels	9
103[d]	1987.07.26	1056	46.89	9.12	1	2.4	90[d]	72[d]	144[d]	193	56	22	145	10	47	38	Steinibach	15
104	1987.10.28	2349	47.08	9.2	7	4.2	178	70	13	84	78	160	132	5	40	23	Mürtschen	15
105	1987.11.01	1016	47.23	9.62	1	2.6	295	78	−169	203	79	−12	159	16	249	1	Feldkirch	15
108	1989.04.02	0658	47.14	9.11	8	3.2	31	43	87	215	47	93	303	2	168	87	Weesen	15
111	1990.11.22	1551	46.89	9	5	3.6	341	60	6	248	85	150	298	17	200	24	Tödi	29
155	1998.04.21	0230	47.14	9.34	10	3.6	209	78	6	118	84	168	164	4	73	13	Walenstadt	24

Table 1. (continued)

FPS	Date	Time	Lat	Lon	z	M_L	First Nodal Plane			Second Nodal Plane			P Axis		T Axis		Location	Ref[a]
							Strike	Dip	Rake	Strike	Dip	Rake	Strike	Dip	Strike	Dip		
Crystalline Massifs																		
C1																		
120	1988.06.11	2244	45.86	6.89	8	3.4	34	50	−174	300	85	−40	249	31	354	23	Mt. Blanc	22
Penninic Nappes (West -1 to East-2)																		
P1																		
115[d]	1985.01.04	1657	46	7.27	10	3.2	329[d]	82[d]	−40[d]	65	50	−170	279	33	23	21	Mauvoisin	22
116	1986.01.19	0654	46.18	7.64	6	3	110	40	−80	277	51	−98	143	82	13	5	Vissoie[b]	22
117	1986.02.15	0143	46.05	7.64	5	3.6	27	70	170	120	80	20	252	7	345	21	Zermatt	22
118	1986.02.26	1307	46.03	7.35	7	2.9	249	51	−133	125	55	−50	94	58	188	2	Dixence	22
119	1987.05.30	1945	45.96	7.91	9	2.7	135	50	−10	231	82	−140	101	33	357	21	Mt. Rosa	22
123	1987.03.22	0136	46.19	7.87	4	2.1	311	51	−47	75	55	−130	286	58	192	2	Stalden	17
127	1990.05.11	0816	46.22	7.77	1	2	263	40	−116	115	55	−70	76	72	191	8	St. Niklaus	17
131	1990.09.25	0519	46.17	7.64	5	3.6	70	50	−130	303	54	−52	273	60	7	2	Vissoie	17
132	1990.12.17	2334	46.22	7.64	5	1.7	319	42	−49	90	60	−120	310	62	201	10	Vissoie[b]	17
133	1991.09.07	1809	46.22	7.94	8	2.4	135	55	−19	236	74	−144	101	37	2	12	Stalden	17
135	1996.03.31	0608	45.94	7.46	4	4.6	44	38	−137	278	65	−60	231	59	347	15	Valpelline	24
156	1998.05.07	1716	46.13	7.39	6	3.3	92	55	−90	272	35	−90	2	80	182	10	Val d'Heremence	24
157	1998.12.09	2208	46.19	7.55	4	3.4	256	28	−80	65	62	−95	323	72	159	17	Grimentz	24
P2																		
102	1987.04.29	2041	46.49	9.82	8	2.6	353	67	−12	88	79	−156	312	24	219	8	St. Moritz	15
106	1988.04.17	0341	46.78	9.47	6	2.2	327	43	−59	108	54	−115	321	69	216	6	Feldis[b]	15
107	1988.05.23	2156	46.73	9.64	7	2.1	345	47	−54	118	54	−122	328	64	230	4	Lenzerheide[b]	15
109	1990.03.18	0954	46.79	9.84	4	3.5	326	38	−38	88	68	−121	317	56	201	17	Davos	15
112[d]	1991.11.20	0154	46.73	9.53	6	5	294[d]	37[d]	−72[d]	92	55	−103	321	76	191	9	Vaz	25

[a]References: 1, *Ahorner et al.* [1972]; 2, *Ahorner and Schneider* [1974]; 3, *Pavoni and Peterschmitt* [1974]; 4, *Pavoni* [1977]; 5, *Fréchet* [1978]; 6, *Thouvenot* [1981]; 7, *Dorel et al.* [1983]; 8, *Jimenez and Pavoni* [1983]; 9, *Pavoni* [1984]; 10, *Deichmann* [1987]; 11, *Pavoni* [1987]; 12, *Sambeth and Pavoni* [1988]; 13, *Deichmann et al.* [2000b] (modified after *Smit* [1989]); 14, *Deichmann* [1990]; 15, *Roth* [1990], *Roth at al.* [1992]; 16, *Bonjer* [1992, 1997]; 17, *Maurer* [1993], *Pavoni et al.* [1997]; 18, *Baer et al.* [1997]; 19, *Fréchet at al.* [1996]; 20, *Plenefisch and Bonjer* [1997]; 21, *Deichmann et al.* [1998]; 22, *Eva et al.* [1998]; 23, *Thouvenot et al.* [1998]; 24, *Baer et al.* [1999]; 25, *Marone* [1999]; 26, *Deichmann et al.* [2000a]; 27, *Deichmann et al.* [2000b]; 28, *Kastrup* [2002], *Fröhlich* [1989]; 29, new fault plane solutions.

[b]FPS has been modified from earlier published solutions.

[c]FPS is a composite solution.

[d]Active fault plane.

published in sources that are not readily accessible are displayed in Figure 3. All events taken from the literature were checked for consistency regarding orientation and orthogonality of the nodal planes. This mainly concerns events recorded prior to 1984. All subsequent events have been studied in detail by various authors (see references in Table 1). Takeoff angles and focal depths were reevaluated by two-dimensional (2-D) ray tracing using the program MODD of *Gebrande* [1976] where it was necessary to account for a laterally heterogeneous crust [e.g., *Eva et al.*, 1998]. The hypocenters of most earthquakes are estimated to be accurate to ±2 km laterally and ±3 km vertically. It was possible to apply cross correlation and precise relative location methods to determine which of the two nodal planes was the fault plane in 20 out of the 138 events [e.g., *Deichmann and Garcia-Fernandez*, 1992; *Roth et al.*, 1992; *Maurer and Deichmann*, 1995]. These planes are marked by the bold line on 20 of the fault plane solutions (FPSs) shown in Figure 2. These 20 events are also identified in Table 1.

[11] The distribution of earthquakes for which a fault plane solution is available is not uniform throughout Switzerland (Figures 1a and 1b). This distribution primarily reflects regional variations in seismic energy release over the period monitored. The scarcity of data is particularly problematic for the stress analysis in the western region of the area studied. Here, besides the low number of events recorded, the uncertainty in the location and fault plane solutions of some of these events is relatively large, since they occurred prior to 1976 when the network was less dense (events 139–142 in Figure 2). For example, the locations of events 141 and 142 are only known to within several tens of km [*Fréchet*, 1978; *Dorel at al.*, 1983]. Thus the FPS of the three events in the western Jura (139, 140, and 142) should be interpreted with caution. Several other events elsewhere also have poor depth constraints, but their fault plane solutions are nonetheless well constrained (39 and 101). The only two events listed in Table 1 which were excluded from the stress inversion owing to a poorly constrained focal mechanism were the 1964 Sarnen event (94) and the earthquake close to St. Blaise in 1979 (146). The overall uncertainty of the focal mechanism parameters is considered to be on average 5°–10°.

[12] Simple inspection of the focal mechanism plots for Switzerland indicates a contrast in deformational style between the foreland in the north and the high Alps to the south (Figures 1b and 2). Whereas most earthquakes in the foreland show a predominantly strike-slip mechanism and some normal faulting, the proportion of normal faulting events increases significantly in the highest and formerly compressional parts of the Alps to the south. Thrust faulting

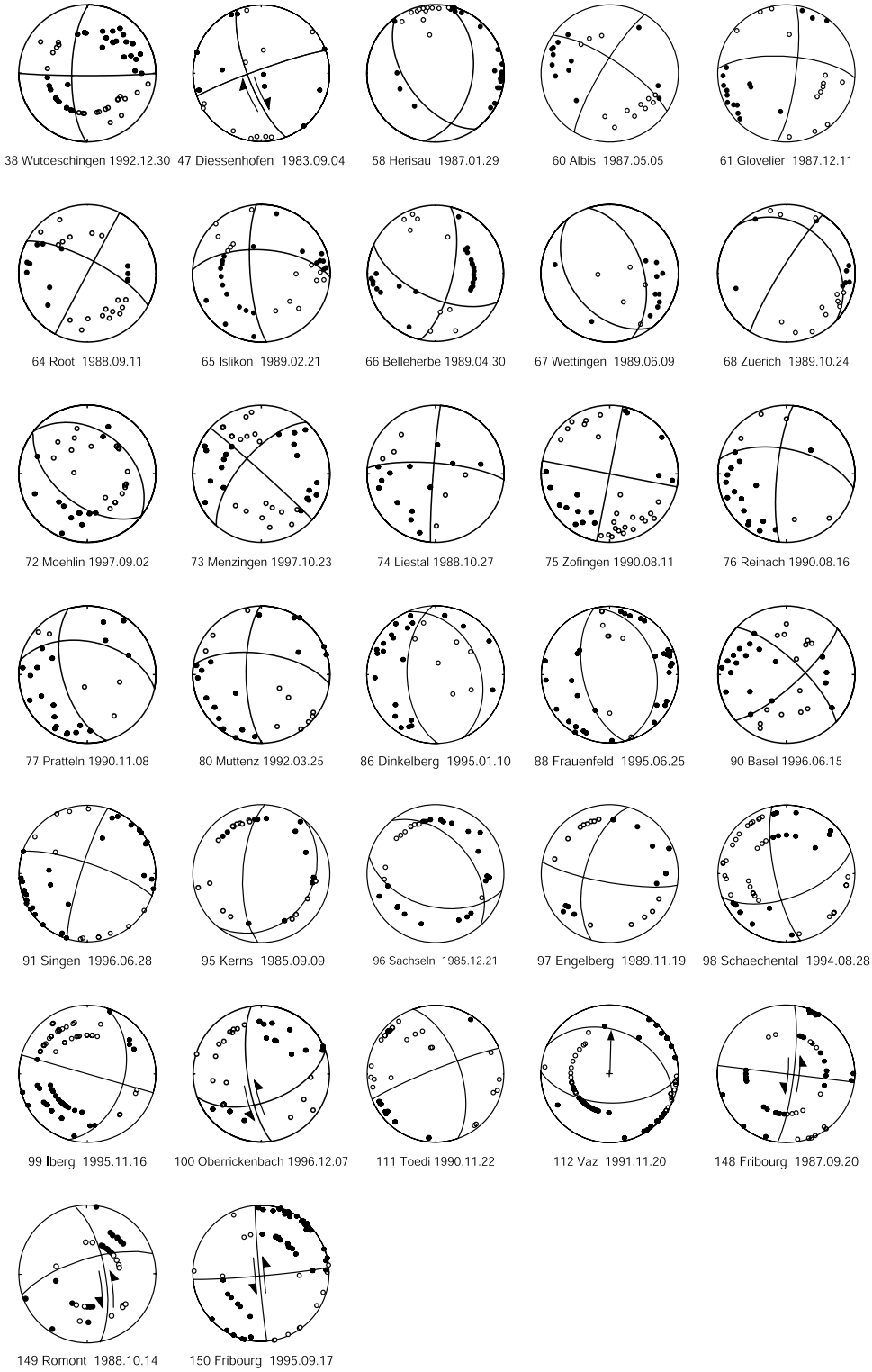

Figure 3. Lower hemisphere, equal-area projection of focal mechanisms used in the study which are currently unpublished or difficult to access. The first motion data points are plotted (solid circles indicate first motion up, and open circles indicate first motion down). Nodal planes known to be the active fault planes are marked by arrows showing the respective motion.

events are occasionally seen in some localities, but are rare. Stereographic plots of the *P* and *T* axes of the events, grouped into the local data subsets we will later use in our stress inversions (Figure 4a), are shown in Figure 4b. They show a progressive counterclockwise rotation of the horizontal component of deformation from east to west in the Alpine foreland and from north to south across the Alps. Thus it is clear that present-day strain is not uniform

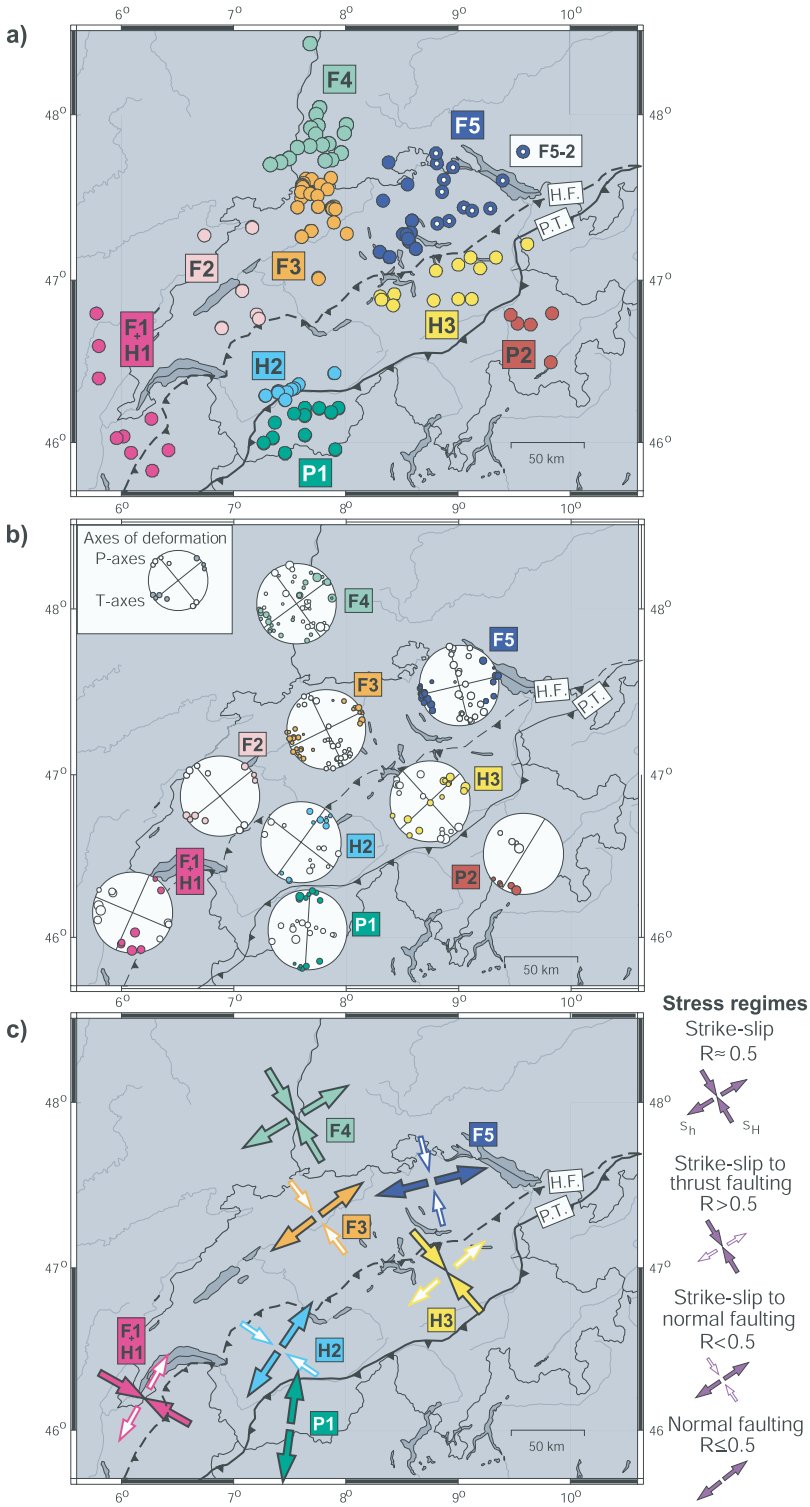

Figure 4. (a) Local groupings of events which were found to yield acceptable stress inversion results (i.e., GF misfit angles <6°). The numbers refer to the different subsets. HF denotes the Helvetic front, and PT denotes the Penninic thrust. The dark blue circles with the small white dot in the center represent a subset of F5, F5-2. (b) Lower hemisphere, equal-area projection of the *P* and *T* axes of the events grouped into the local data subsets used for the stress inversions. The open and solid circles denote the *P* and *T* axes, respectively, and the size of the circles is magnitude-dependent. The lines indicate the mean direction (azimuth) of the *P* and *T* axes of the groups. In all but two cases (F2 and P2), each data group could be inverted to obtain a meaningful estimate of the stress field. (c) Summary of results of the stress inversions of the data sets shown in Figure 4a. See legend for explanation of the arrows.

throughout Switzerland, and it is of interest to determine how these variations are expressed in terms of stress.

4. Stress Inversion Methods

[13] Subsets of the 138 fault plane solutions were inverted to estimate the regional deviatoric stress tensors in Switzerland using the two most commonly used methods developed by *Gephart and Forsyth* [1984] (hereinafter referred to as GF), *Gephart* [1990], and by *Michael* [1984, 1987]. Both methods search for the stress tensor which brings the shear tractions resolved on the fault planes into alignment with the corresponding slip directions (i.e., rake) of the fault plane solutions. The parameters solved for in the inversions are the orientation of the principal stress axes, S_1, S_2, and S_3 (with $S_1 > S_2 > S_3$ under the compression-positive stress convention) and the value of the stress deviator, $R = (S_2 - S_1)/(S_3 - S_1)$, [e.g., *Etchecopar et al.*, 1981]. Thus the inversion constrains the shape and orientation of the stress ellipsoid but yields no information about the absolute magnitude of the stresses.

[14] We applied both methods because they are based on slightly different assumptions and use different inversion strategies [*Gephart*, 1990; *Michael*, 1984, 1987] (for comparison, see *Kastrup* [2002]). Runs with GF's program were initially performed using a 10° grid and a range of 90° (search of the whole grid). Those data sets, which yielded results indicating a uniform stress state, were reevaluated with a 5° grid, which usually tightened the confidence limits. R was searched over the range from 0 to 1 in steps of 0.05. Two runs were made for each data set with the 10° grid: the first with no plane specified as the active fault plane, and the second with the active plane specified for all events in the data set for which it was known. Additional remarks to GF's method are made by *Kastrup* [2002]. In this paper we report only results obtained using the 5° grid with the known fault planes specified. For the inversions with Michael's program, three different approaches were tried. These approaches differ primarily in the implementation of the bootstrapping method to compute confidence limits. A detailed comparison of the results is given in *Kastrup* [2002]. Here we present only the results obtained with the method referred to by *Kastrup* [2002] as Bootstrap variant 2. In this method, which is closest to that proposed by *Michael* [1987], the bootstrap process repeatedly selects a subset of planes at random from a data set that contains all active fault planes from events where they are known and all nodal planes from events where the fault planes are not known. All planes in the data set are assigned the same probability of being selected, perhaps more than once. The computation of confidence limits in the bootstrapping method requires that a best fit solution be defined in order to serve as a reference vector from which distances (in a vector space sense) of solutions can be computed. The best fit solution that we use is obtained by inverting the set of planes identified by GF's method as the set that yields the lowest misfit (one plane for each event). The use of GF's method to identify the collection of planes most likely to have failed in the earthquakes is a rational approach in situations where a choice cannot be made on the basis of relative hypocentral locations or of structural information [*Kastrup*, 2002]. In this way, both best fit inversions use the same set of planes as input, and thus the effect of the different assumptions and procedures inherent in the methods can be judged by simply comparing solutions.

[15] Comparison of the results presented in Table 2 and Figure 5 shows that whereas both methods yield similar estimates for the best fitting stress tensors, they differ radically in the estimated confidence limits. Confidence limits derived from *Gephart and Forsyth*'s [1984] method are generally larger than those obtained from *Michael*'s [1984, 1987] method. *Hardebeck and Hauksson* [2001], in their comparative study based on synthetic focal mechanism data with random errors, found that Michael's confidence regions are usually correct while GF's are too large. The discrepancy in the size of the confidence regions was sometimes important in deciding whether changes in stress between neighboring regions were resolved in Switzerland. Thus the matter is discussed at some length by *Kastrup* [2002]. Following *Hardebeck and Hauksson*'s [2001] results, our interpretations rely on the confidence limits obtained from Michael's method. However, recognizing that the reasons for the discrepancy are not understood, we present the results from both methods.

[16] The resolution of the R value is poor in comparison to the orientation of the principal stress axes. *Hardebeck and Hauksson* [2001] also found that GF's estimates for R are unreliable for the case in which the stress state is actually axisymmetric (i.e., $R = 0$ or 1). In such situations, the best fit solution tends to a value of 0.5, and the confidence limits are too small, in contrast to the more general nonaxisymmetric situation, where the confidence limits tend to be too large. This also turned out to be a problem in this study. Nonetheless, in most cases the R value is sufficiently well resolved to determine whether R is greater than or less than 0.5 (i.e., whether the magnitude of S_2 is closer to S_1 or S_3).

[17] Numerous inversions were run with varying subsets of the whole data set to evaluate whether the stress field in any two neighboring regions is significantly different. The average misfit of the best fit solution obtained from GF's method was used as a discriminator: following *Wyss et al.* [1992], data sets which yield an average misfit of >6°fs were rejected as containing too great a mean error in the FPSs, or as stemming from a data volume in which stress is not homogeneous [*Kastrup*, 2002]. If possible, we tried to reduce the average misfit to <4°. If the GF misfits and stress tensors obtained from the inversion of subsets of a data set yield the same result as the combined data set, the stress field is considered to be homogeneous. The stress states of two adjacent regions are considered different if the 95% confidence regions obtained from *Michael*'s [1984, 1987] method around any one of the principal stress axis orientations or around the R value do not overlap.

5. Results

[18] The 138 fault plane solutions were divided into the nine regionally distinct data sets shown in Figure 4a. There are five data sets in the foreland, two in the Helvetic nappes, and two in the Penninic nappes. The choice of subdivisions within these three principal structural units was unavoidably influenced by the natural clustering of the events. Nonetheless, the coverage is sufficient to determine whether

Table 2. Results of the Inversion Runs Obtained With the *Gephart and Forsyth*'s [1984] and *Michael*'s [1984] Algorithm (Lower Hemisphere Schmidt Net)[a]

Regional Data Set	FPS/Thereof Known Active FPs	Misfit	Plunge/Azimuth S_1	Plunge/Azimuth S_2	Plunge/Azimuth S_3	PHI	R
			10° Grid				
All FPS	138/19	9.652	10/123	77/343	8/215	80.3	0.7
			5° Grid				
Foreland							
F2 + F3	36/8	6.134	59/351	26/135	16/233	−27.2	0.5
F3	29/5	5.043	16/136	61/14	23/233	72.7	0.65
F3 (M)	29/5	14	22/147	65/357	11/242		0.4
F4	30/0	6.890	2/145	83/40	6/235	88.3	0.5
F4 (M)	30/0	21	5/142	85/346	2/233		0.41
F5	24/3	4.819	5/169	82/297	6/79	−85.3	0.4
F5 (M)	24/3	14	8/165	82/336	1/75		0.26
F5-2	11/3	2.824	48/153	42/343	5/249	42.0	0.2
F5-2 (M)	11/3	12	40/164	50/347	1/256		0.06
Different depth ranges (Foreland only)							
			10–15 km				
10 < F4 < 15	15/0	4.729	15/324	62/84	23/228	−73.9	0.2
10 < F4 < 15 (M)	15/0	23	14/141	76/333	3/232		0.33
			<15 km				
F3 < 15	17/5	4.625	17/133	69/349	12/226	72.5	0.5
F3 < 15 (M)	17/5	23	33/139	56/335	7/234		0.33
F5 < 15	10/3	4.021	5/159	78/275	10/68	−84.7	0.5
F5 < 15 (M)	10/3	16	8/171	82/329	3/81		0.35
			>15 km				
F3 > 15	12/1	3.196	36/347	46/209	22/94	50.6	0.2
F3 > 15 (M)	12/1	18	85/168	4/350	0/260		0.06
F5 > 15	14/0	3.029	77/178	12/341	4/71	−12.0	0.3
F5 > 15 (M)	14/0	6	71/167	18/337	3/68		0.24
			15–20 km				
15 < F4 < 20	9/0	3.436	61/330	29/150	0/60	29.3	0.3
15 < F4 < 20 (M)	9/0	25	37/327	53/141	3/235		0.32
			<20 km				
F2 + F3 < 20	28/8	6.007	59/348	27/138	13/235	−28.2	0.45
(M) F2 + F3 < 20	28/8	16	43/341	46/143	9/242		0.14
F3 < 20	23/5	4.849	20/134	59/7	23/233	68.2	0.6
F3 < 20 (M)	23/5	18	25/139	62/350	13/235		0.37
F5 < 20	12/3	4.819	6/155	79/278	9/64	−83.9	0.45
F5 < 20 (M)	12/3	18	3/168	85/297	4/77		0.25
			>20 km				
F3 > 20	6/0	1.789	15/323	48/216	38/65	71.3	0.7
F3 > 20 (M)	6/0	19	7/320	78/202	10/57		0.5
F5 > 20	12/0	2.207	5/169	82/297	6/79	−85.3	0.4
F5 > 20 (M)	12/0	18	49/150	39/349	9/251		0.3
Foreland and Helvetic nappes							
F1 + H1	8/1	1.710	11/127	70/3	16/220	−74.0	0.6
F1 + H1 (M)	8/1	13	8/294	78/69	8/203		0.88
Helvetic nappes							
H2	10/3	3.213	23/301	54/175	26/43	63.9	0.35
H2 (M)	10/3	9	14/302	70/169	14/35		0.24
H3	13/2	5.422	2/158	16/67	74/256	−16.1	0.15
H3 (M)	13/2	24	3/318	56/223	34/59		0.9
Pennic nappes							
P1	13/1	2.119	75/209	5/101	14/10	4.9	0.35
P1 (M)	13/1	6	75/246	12/103	9/12		0.32

[a]Regional data set (see Figure 4a) (numbers connected by a plus refer to combined data sets); (M) refers to the inversion results run with Michael's inversion scheme; amount of inverted focal mechanisms (first number) and the amount of focal mechanisms thereof for which the active fault plane is known; misfit of the best stress tensor; plunge and azimuth of S_1 (best stress tensor); plunge and azimuth of S_2 (best stress tensor); plunge and azimuth of S_3 (best stress tensor); PHI value (following GF's definition) of the best stress tensor (angle between S_1 and the vertical axis in the plane perpendicular to S_3; R value ($S_2 - S_1/S_3 - S_1$) of the best stress tensor.

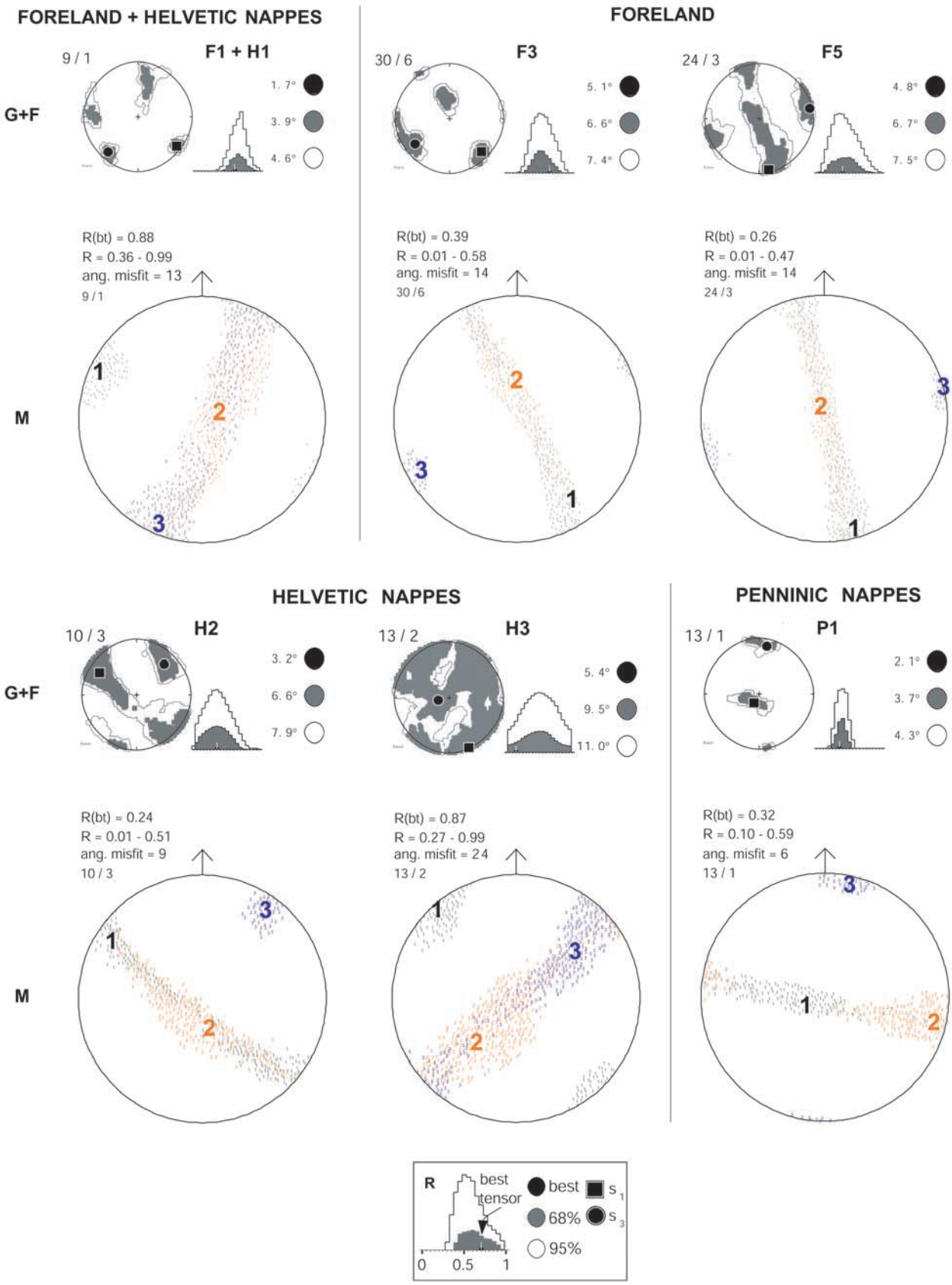
FORELAND + HELVETIC NAPPES
FORELAND
HELVETIC NAPPES
PENNINIC NAPPES
G+F
M
9 / 1
F1 + H1
1. 7°
3. 9°
4. 6°
30 / 6
F3
5. 1°
6. 6°
7. 4°
24 / 3
F5
4. 8°
6. 7°
7. 5°
R(bt) = 0.88
R = 0.36 - 0.99
ang. misfit = 13
9 / 1
R(bt) = 0.39
R = 0.01 - 0.58
ang. misfit = 14
30 /6
R(bt) = 0.26
R = 0.01 - 0.47
ang. misfit = 14
24 /3
10 / 3
H2
3. 2°
6. 6°
7. 9°
13 / 2
H3
5. 4°
9. 5°
11. 0°
13 / 1
P1
2. 1°
3. 7°
4. 3°
R(bt) = 0.24
R = 0.01 - 0.51
ang. misfit = 9
10 / 3
R(bt) = 0.87
R = 0.27 - 0.99
ang. misfit = 24
13 / 2
R(bt) = 0.32
R = 0.10 - 0.59
ang. misfit = 6
13 / 1
R
best tensor
0
0.5
1
best
68%
95%
s1
s3

systematic changes in stress occur, and whether they correlate with such variables as topography and crustal thickness.

[19] Comparison of best fit solutions from the GF and Michael methods in Table 2 shows that the orientations of the stress axes are generally in accord, indicating that the different assumptions and methodologies inherent in the two methods do not have a significant effect on the solutions. The 95% confidence limit contours obtained from the Michael (variant 2) method usually matches the 68% contours obtained from the GF method closely. Michael's method is preferred in situations where GF's method of selecting the fault plane is prone to error. This is the case when the magnitude of two of the principal stresses is similar (axisymmetric stress state), and when the difference between the two misfit angles of the individual nodal planes of an event for the best fit solution is small.

[20] The results confirm the expectation that the stress regime in Switzerland is characterized by a strike-slip to normal faulting regime with S_3 subhorizontal. Thus for most data sets, S_3 represents the minimum horizontal stress, S_h (Figures 4c and 5 and Table 2). More importantly, the orientation of S_3 is usually much better constrained and more stable than the orientation of either S_1 or S_2. Indeed, the best fit solutions for S_1 and S_2 vary greatly between neighboring data sets, and their 95% confidence limits from both methods commonly overlap, forming a band across the stereonet in the plane perpendicular to S_3. Exceptions to this behavior are the inversion results for the data sets in the southwest (F1 + H1) and in central Switzerland (H3), where a few thrust mechanisms cause an overlap of the orientations of S_2 and S_3 (Figure 5).

[21] Two distinct trends in stress are evident: one trending north-south and the other northeast-southwest, or approximately normal and parallel to the Alpine mountain belt. (Figure 4c).

5.1. Variation of Stress Along the Strike of the Alpine Chain

[22] Here we examine the variation of stress along the Alpine chain within each of the three main structural units (foreland, Helvetic nappes, and Penninic nappes). In the foreland, north of the Helvetic front, the pattern of stress variations from east to west is best seen in the results of *Michael*'s [1984, 1987] method applied to data sets F1+H1, F3 and F5 (Figure 5 and Table 3). The GF misfit of the best fit solution for each of these data sets is less than 6°, and thus they are considered to define zones within which the stress is acceptably uniform. Smaller misfits were obtained for local subsets of the F5 data set (e.g., F5-2 in Figure 6), which might indicate some degree of stress heterogeneity within the F5 data region (see section 4 and *Kastrup* [2002]). However, the corresponding stress descriptions were largely the same, and hence, for simplicity, we work with the lumped data set (F5). The results from both methods show that the F3 and F5 regions are characterized by a strike-slip/normal fault stress regime with S_3 subhorizontal, and S_1 and S_2 orientations unconstrained within a band normal to S_3. This suggests that S_1 and S_2 are approximately equal in magnitude. Both methods also indicate a counterclockwise rotation in S_3 orientation from east (F5) to west (F3). This rotation of some 25° is just resolved at Michael's 95% confidence limits, but not at GF's 68% limits. However, if the extreme southwest foreland region F1 + H1 (which lies entirely in France and includes seven foreland earthquakes augmented by two events in the Helvetic realm) is included, the net S_h rotation across the arc of the foreland, from F5 to F1 + H1, increases to 40°–50°, and is resolved by both methods. The increase in the rotation of S_h direction around the arc is progressive. This is seen most clearly in the P and T axes plot of Figure 4b, which includes the data from region F2 where there are too few data with different mechanisms to perform a formal stress inversion. The strong rotation in S_h orientation that occurs between regions F3 and F1 + H1 is accompanied by a change in the stress regime from strike-slip/normal (F3) to strike-slip/thrust (F1 + H1). This is indicated most clearly by the results of Michael's method for F1+H1 where the 95% confidence limits for S_2 and S_3 are unconstrained within a band normal to S_1, indicating the magnitudes of S_2 and S_3 are similar (for F3, the band extends between S_1 and S_2). It is also indicated by the contrast in R values obtained from Michael's method, which tend to be significantly larger for F1 + H1 than F3 or F5 (Figure 5).

[23] The results for the southern Rhine Graben data set (F4) are consistent with those obtained by *Plenefisch and Bonjer* [1997] for the same region and will thus not be discussed here (for details, see *Kastrup* [2002]).

Table 3. Stress Inversion Results Using Michael's and Gephart and Forsyth's Method for Foreland Data Sets Along the Strike of the Alpine Arc

Region	Data Set	S_1 Axis Dip/Azimuth	S_3 Axis Dip/Azimuth	S_h Azimuth
Northeastern foreland				
Gephart and Forsyth	F5	5/169	6/79	N79°E
Michael		8/165	1/75	N75°E
Northern foreland				
Gephart and Forsyth	F3	16/136	23/233	N46°E
Michael		22/147	11/242	N62°E
Southwestern foreland				
Gephart and Forsyth	F1 + H1	11/127	16/220	N37°E
Michael		8/294	8/203	N23°E

Figure 5. Stress inversion results for the foreland, Helvetic, and Penninic data sets (F1 + H1 actually also includes two data from the Helvetic nappes). (top) Results from *Gephart and Forsyth*'s [1984] method, where contours of the 68% (grey) and 95% (white) confidence regions about the best fit solution are shown for the orientation of S_1 (square) and S_3 (circle). The unnormalized probability density functions (pdf) of the corresponding R values are shown to the right of the stereonet together with the misfit values associated with the confidence contours. (bottom) Results from *Michael*'s [1987] method. The orientations of all three stress axes obtained from each bootstrap run are plotted for all solutions that lie within the 95% confidence limits, and the best fit values indicated by the large bold numbers. The corresponding range of R values and the best fit value are indicated above the stereonet, as is the misfit angle (not the same angle as the GF misfit). Both stereonets use a lower hemisphere, Schmidt projection. See text for further discussion.

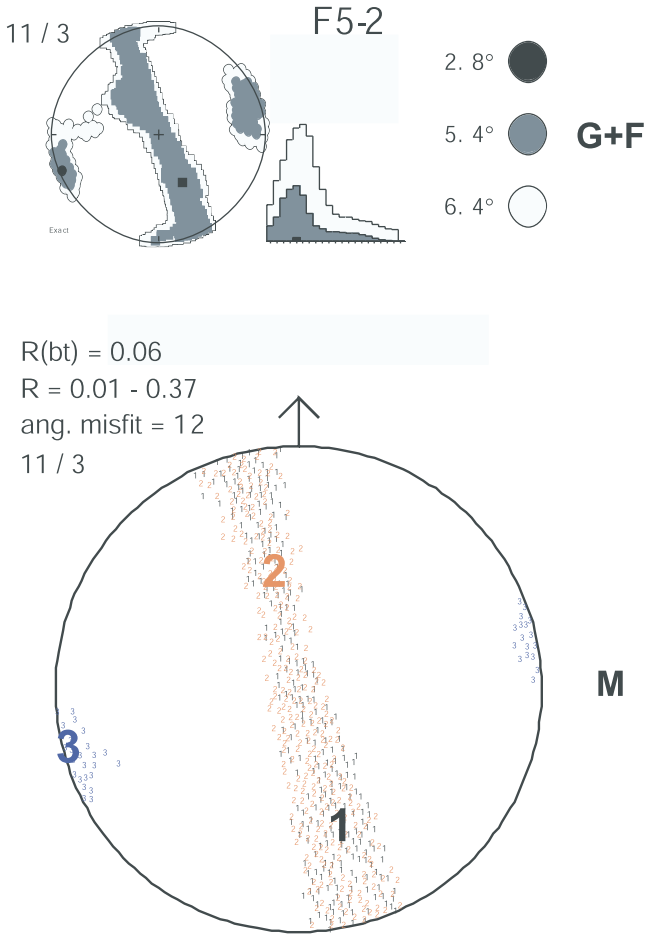

Figure 6. Stress inversion results for data set F5-2 which is a subset of F5 that has a lower Gephart and Forsyth average misfit angle. The inclination of S_1 is unconstrained, lying anywhere within a band normal to S_3, as is the case for the F5 inversion results in Figure 5.

[24] The variation in stress along the structural strike within the Helvetic nappes is given by the results from regions H2 and H3 shown in Figure 5. In the southwest (H2), both methods indicate that S_3 is oriented NE-SW, and is well constrained and subhorizontal. S_1 and S_2 are largely unconstrained within the plane normal to S_3, implying a predominantly strike-slip regime with a normal faulting component. In the northeast (H3), the orientation of S_3 is also NE-SW, with no rotation relative to its orientation in H2 resolved at Michael's 95% confidence level. However, in H3, S_3 is unconstrained within a vertical band formed with S_2, indicating a strike slip to thrust faulting regime (only resolved with Michael's method). This change in the stress regime along the arc, even though not resolved at the 95% confidence limits is also reflected in the R values obtained from Michael's method. Specifically, although no difference in R value is resolved at the 95% confidence limit, the R values tend to be larger than 0.5 in the northeast and less than 0.5 in the southwest, indicating a bias toward thrust faulting ($S_2 = S_v$ closer to S_3) in the northeast and normal faulting in the southwest ($S_2 = S_v$ closer to S_1). Examination of the fault plane solutions supports this contention: many events in the northeast display a significant thrust component (e.g., FPS 95, 98, 100, 103, 108 in Figure 2), whereas those in the southwest tend to display a larger normal faulting component.

[25] The variation in the state of stress along the strike of the Penninic nappes is obscured by the poor resolution of the stress axes obtained for the Graubünden (P2) data set in the east. This is due to a lack of diversity in the focal mechanism solutions available for that region. Nevertheless, the fault plane solutions themselves indicate that the style of ongoing deformation in the eastern Penninic nappes is similar to that in the western Penninic nappes in southern Wallis (data set P1), except for an apparent counterclockwise rotation of some 25°. This can be seen from the plots of P and T axes of events from the P1 and P2 regions shown in Figure 4b, suggesting that the orientation of S_h is similarly rotated. In any case, we conclude that the ongoing deformation, and possibly the stresses, in Graubünden appears to involve extension toward ~30°N and thus strikes obliquely at ~45° to the local trend of the Alps (75°N).

[26] Variations of stress with depth were examined in the northern foreland by analyzing the data for focal depths less than and greater than 15 km separately. The rotation along strike of the Alps seems to be less pronounced for the deeper events than for the shallower events. However, as the 95% confidence limits overlap and there are no lower crustal events in the southwest, a significant variation of the stress field with depth in the northern foreland is not sufficiently well constrained by the available data [*Kastrup*, 2002].

5.2. Variation of Stress Across the Strike of the Alpine Chain

[27] Here we examine the variation in stress along profiles normal to the Alpine chain in eastern and western Switzerland. The available data in eastern Switzerland is limited to the results obtained by Michael's method and concerns only the foreland and the Helvetic nappes, owing to the poor resolution of stress in the eastern Penninic nappes (P2). Stress in the eastern foreland is characterized by the results from data set F5, while the relevant data set in the Helvetic nappes is H3. North of the Helvetic front, S_3 is oriented approximately ENE-WSW, whereas to the south (H3) it is more NE-SW oriented (Figure 5), implying a counterclockwise rotation of up to 30° resolved at Michael's 95% confidence limits. This is accompanied by a change in R value across the Alpine front with values tending to be less than 0.5 in the north and greater than 0.5 in the south (according to estimates from Michael's method). Even though the 95% confidence limits overlap, this change can also be traced with the best fit R values. This implies a change in stress regime from strike-slip/normal faulting in the eastern foreland to strike-slip/thrust faulting in the eastern Helvetic nappes. As noted earlier, the significant component of thrust faulting in the latter region is also evident in the fault plane solutions in Figure 2.

[28] For the eastern Penninic nappes, we can only refer to the mean axis of deformation (Figure 4b) to evaluate differences with respect to the Helvetic nappes. Also here, a 20° counterclockwise rotation in S_h orientation from north to south is suggested, accompanied by a change in deformation style from thrust/strike slip faulting in the Helvetic nappes to normal faulting in the Penninic nappes.

Table 4. Stress Inversion Results Using Michael's and Gephart and Forsyth's Method for Data Sets That Define the Western Profile Across the Alpine Belt

Region	Data Set	S_1 Axis Dip/Azimuth	S_3 Axis Dip/Azimuth	S_h Azimuth
Northern foreland				
Gephart and Forsyth	F3	16/136	23/233	N46°E
Michael		22/147	11/242	N62°E
Northern Wallis				
Gephart and Forsyth	H2	23/301	26/43	N31°E
Michael		14/302	14/35	N35°E
Southern Wallis				
Gephart and Forsyth	P1	75/209	14/10	N10°E
Michael		75/246	9/12	N12°E

[29] The data in western Switzerland provide a complete NNW-SSE profile of the state of stress across the three main structural units. The relevant data sets from north to south are F3, H2, and P1. The stress inversion results for these regions are listed in Table 4. Comparison of the results from Michael's method in Figure 5 shows that a well-resolved 20°–25° counterclockwise rotation in S_3 orientation occurs between each of these three units from north to south. The results from GF's method confirm the S_3 rotation between the Helvetic and Penninic nappes, but the rotation between the Helvetic nappes and the foreland is not strictly resolved. However, comparison of the F3 and H2 stereonets in Figure 5 shows that the GF 68% confidence regions appear rotated by about 20° with respect to each other. This further supports our interpretation, based on the results obtained with Michael's algorithm, that the rotation is real. The horizontal stress rotation between the Helvetic and Penninic nappes is also accompanied by a change from strike-slip/normal faulting in the north (S_1 horizontal or vertical) to predominantly normal faulting in the Penninic nappes (S_1 predominantly vertical). No change in faulting regime is evident in the west between the Helvetic nappes and the foreland.

[30] Thus both in western and in eastern Switzerland we observe a counterclockwise horizontal rotation of the stress axes of 40°–45° from the Alpine foreland to the Penninic nappes, with largely strike-slip deformation in the north giving way to extensional deformation in the Penninic nappes.

5.3. Ambiguity in S_1 Inclination: Similarity in the Magnitude of S_1 and S_2?

[31] Most of the results in the foreland indicate that the inclinations of S_1 and S_2 are poorly constrained: the 95% confidence limits from both methods extend across the stereonet as a band in the plane normal to S_3. *Plenefisch and Bonjer* [1997] and *Evans and Roth* [1998] also inverted data sets from the central foreland using GF's method and obtained similar results. There are two possible explanations for the ambiguity in S_1 inclination that we mention.

[32] One explanation is that the ambiguity in S_1 inclination reflects stress heterogeneity within the data volumes. While we cannot wholly discount this owing to the difficulty in estimating heterogeneity, we note that the same ambiguity is seen in the results of inversions of subsets of the data, when very small GF misfits are obtained. An example is presented in Figure 6 where we show the results of inverting a local subset of data from region F5 (referred to as F5-2 and indicated on Figure 4a). The GF misfit angle for the best fit solution is only 2.8°. Thus we consider stress heterogeneity to be an unlikely explanation.

[33] The second and simpler explanation is that the magnitudes of S_1 and S_2 are similar. This necessarily implies that the R value must be close to zero. *Plenefisch and Bonjer* [1997] and *Evans and Roth* [1998] both found R values close to 0.5 and the latter remarked that this was inconsistent with $S_1 = S_2$. Examination of the R values from our inversions of the northwestern and northeastern foreland data sets (Figures 5 and 6 and Tables 2 and 5) shows that the 95% confidence regions for R obtained from Michael's method (or 68% for GF's) are mostly in the 0–0.5 range, with best fit values from Michael's method tending to the lower end of this range and those from GF's method to the higher. *Hardebeck and Hauksson* [2001] suggest that the R value estimates from GF's method are unreliable when the stress state is close to axisymmetric (e.g., $S_1 = S_2$). Nonetheless, to better understand the resolution of R value, we examined whether the R-value confidence estimates vary with S_1 orientation (i.e., whether the distributions of acceptable values for S_1 and R are correlated). Therefore we plotted the 68% and 95% confidence regions (contours of equal misfit) of S_1 and R for all GF solutions of data set F5-2 that lie in the plane normal to the best fit value of S_3 (Figure 7). The distribution of R-values is essentially independent of the orientation of S_1, demonstrating that the two are not correlated. Thus we conclude that the ambiguity in S_1 orientation that characterizes the northeastern and northwestern foreland probably reflects a similarity in the magnitude of S_1 and S_2.

6. Possible Explanations for Stress Field Variations

[34] In this section we examine the correlation between the resolved variations in stress regime and potential causes such as topography, Moho depth, major tectonic structures, inden-

Table 5. Comparison of Misfits and R Values for the Results Obtained With Gephart and Forsyth's Method and Michael's Bootstrap Variant 2 Method

	Misfit Associated With the Best Fit Solution		Best Fit R Value		Limits of R Values		
Regional Data Set	GF	Michael Variant 2	GF	Michael Variant 2	GF (68%)	Michael 95%	Comments
F1 + H1	1.7	13	0.6	0.88	0.45–0.9	0.36–0.99	possibly axisymmetric ($S_2 = S_3$)
F3	5.1	14	0.65	0.4	0.3–0.8	0.01–0.58	possibly axisymmetric ($S_1 = S_2$)
F5	4.8	14	0.4	0.26	0.1–0.85	0.01–0.47	possibly axisymmetric ($S_1 = S_2$)
F5-2	2.8	12	0.2	0.06	0.0–0.9	0.01 – 0.37	axisymmetric ($S_1 = S_2$)
H2	3.2	9	0.35	0.24	0.0–0.75	0.01–0.51	possibly axisymmetric ($S_1 = S_2$)
H3	5.4	24	0.1	0.87	0.0–1.0	0.27–0.99	possibly axisymmetric ($S_2 = S_3$)
P1	2.1	6	0.35	0.32	0.25–0.5	0.1–0.59	

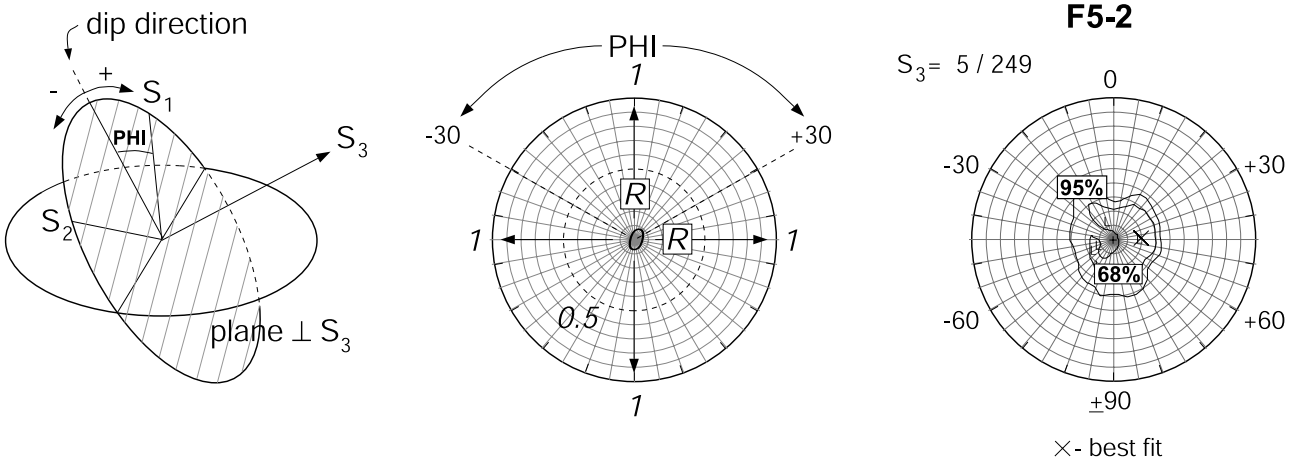

Figure 7. Polar plot of GF solution space for the inversion of F5-2, which shows how the R values (radial axis with range 0–1) obtained in the solutions vary as a function of S_1 orientation within the plane normal to S_3. The latter is measured by the angle PHI which is the rake of S_1 in the plane normal to S_3. Plotted are contours of PHI and S_1 for solutions that bound the 68% and 95% confidence regions (i.e., contours of equal misfit angle).

tation of the Adriatic microplate, and crustal thickness. To this end, we place our results in a larger regional context that also includes stress field estimates from other studies (Figure 8).

6.1. Changes in the State of Stress Along the Strike of the Alpine Chain

[35] The rotation in the horizontal stresses of 40°–50° around the foreland of Alpine chain described above is also seen in paleostress data from the Jura Mountains (3–5 Ma) and the Molasse Basin (11–26 Ma) [e.g., *Laubscher*, 1972; *Becker*, 2000, and references therein] and in the pattern of P and T axes [*Pavoni*, 1980, 1987, 1992] (Figure 4b). It is not evident in near-surface stress measurement data from the northern Alpine foreland which indicate large local variations in minimum principal horizontal stress orientation [e.g., *Becker et al.*, 1987; *Becker*, 1999, 2000; *Evans and Roth*, 1998, and references therein]. However, this variability probably reflects the structural complexity of the upper 2–5 km. The low misfits of our results suggest that the degree of stress heterogeneity in the deeper basement where the earthquakes occur is less pronounced, even for the region at intersection of the foreland with the Rhine Graben (data set F3) where a major structural disturbance to the basement is found [*Mayer et al.*, 1997].

[36] The most relevant observation in our view is that the rotation follows the curvature of the Alpine arc, and that it is only observed in the vicinity of the Alps (Figure 8). At greater distance, basically beyond the foreland, it melts away into the rather uniform NW-SE compressional stress field of Western Europe that is probably related to the push from the North Atlantic Ridge and to the convergence between Africa and Europe [*Müller et al.*, 1992]. Thus this rotation reflects a stress perturbation, remnant or active, arising from the processes of Alpine collision, and which is defined at the scale of the Alpine arc. It follows that its cause must also be coherent on the scale of the Alpine arc. There are two candidate mechanisms that act at this scale: rigid indentation by a plate, and large-scale perturbation of crustal and lithospheric thickness.

[37] *Pavoni* [1961] first proposed that the rotation reflected stresses arising from the indentation of a rigid body into a viscoelastic material. *Grünthal and Stromeyer* [1992] and *Regenauer-Lieb and Petit* [1997] used conceptually similar models to show that the observations are consistent with the expected rotation of the stresses around the corner of the indenting Adriatic plate. On the basis of their results, *Regenauer-Lieb and Petit* [1997] proposed that at present, the entire Central European plate gives way to the penetrating Italy/Adria Block by a NE-SW extension mechanism and a volume flux into the Mediterranean to the west of the Alps, a hypothesis that can explain why the NE-SW orientation of S_3 is the most stable facet of the stress field throughout the foreland.

[38] An alternative explanation is that the along-strike stress rotation reflects the effect of buoyancy forces arising from the 3-D structure of the Moho (Figure 8) and perhaps an underlying lithospheric root. This mechanism is described in detail in section 6.2.1, where it is invoked to explain the across-strike variations in horizontal principal stress orientation. At first sight it seems improbable that the along-strike stress rotation can be due to variations in Moho depth or surface topography since both are more or less uniform along the foreland in Switzerland. However, as Figure 8 shows, the deviation for 2-D uniformity of Moho depth into the strongly 3-D, arcuate form in the western Alps has already occurred in the region of our westernmost data set F1 + H1, where the rotation was most clearly manifest. However, significant rotation is also seen eastward of this point around the arc where the Moho is more 2-D (Figures 4b and 4c). It remains for future geodynamical modeling to evaluate whether the 3-D structure of the Moho in the west can account for the observed along-strike rotation in stresses in the east.

6.2. Changes in the State of Stress Across the Alpine Chain

[39] Deformation in the Penninic domain differs from that in the rest of Switzerland by displaying a larger component

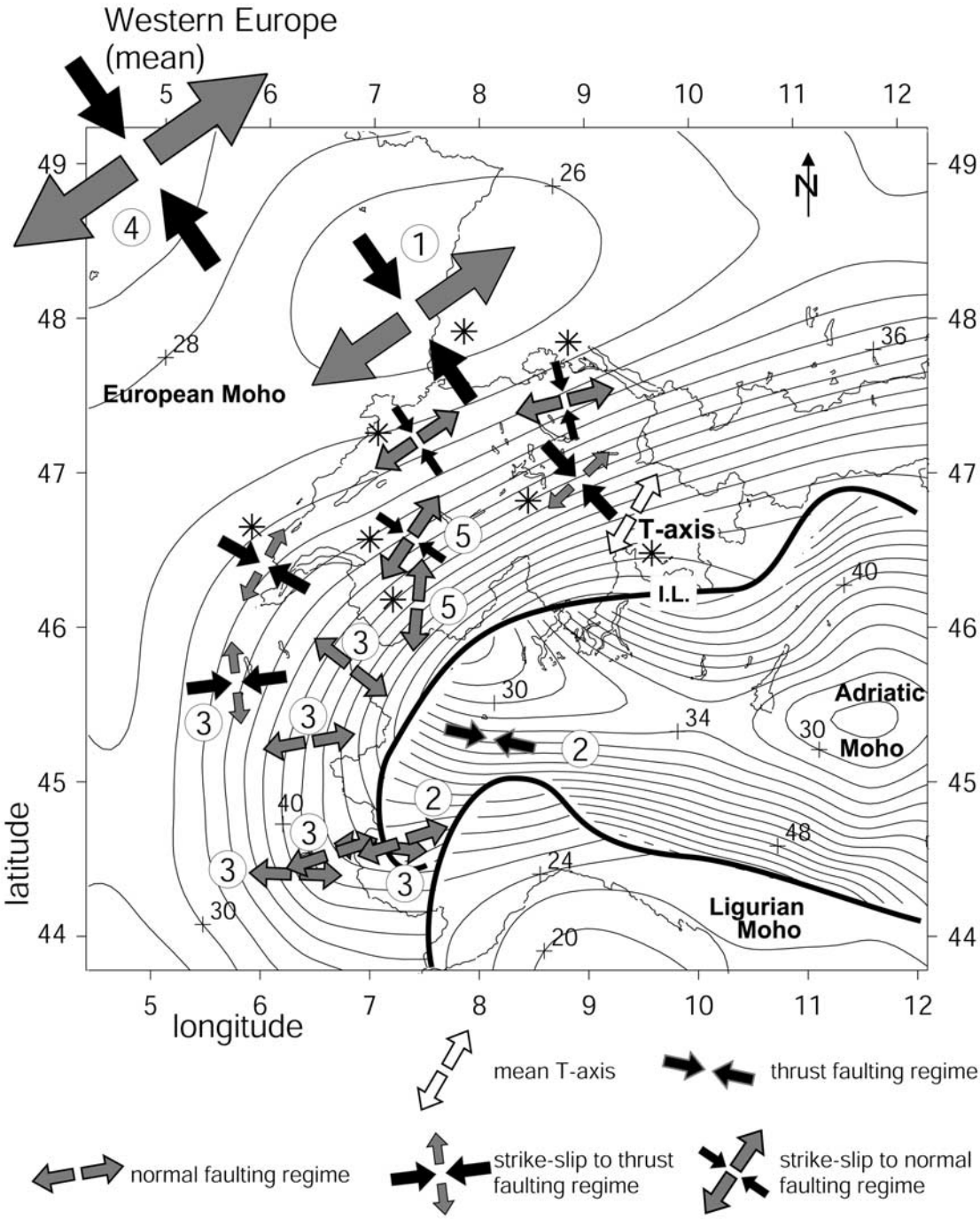

Figure 8. Summary of stress state determinations from this and other studies shown with the depth to Moho in the Alpine region after *Waldhauser et al.* [1998]. The contour interval is 2 km. Stress determinations without a number are from this study (Figure 6). The other data are derived from the following sources: 1, *Bonjer et al.* [1984], *Larroque et al.* [1987], *Carey-Gailhardis and Mercier* [1992], *Delouis et al.* [1993], *Maurer et al.* [1997], *Plenefisch and Bonjer* [1997], and *Evans and Roth* [1998]; 2, *Eva et al.* [1997]; 3, *Sue at al.* [1999]; 4, *Müller et al.* [1992]. The "first-order" stress state prevailing over most of western Europe is shown beyond the Alpine foreland in the top left corner.

of normal faulting accompanied by the counterclockwise rotation of the horizontal stresses by about 20°–25° with respect to the Helvetic nappes, and 40°–50° with respect to the foreland regions. *Roth* [1986] and *Maurer et al.* [1997] both proposed that different stress regimes exist in the northern and southern Wallis. Our results confirm their assertion, and further suggest that the Helvetic nappes represent a transition zone between the contrasting stress regimes in the Penninic nappes and the foreland. The vertical orientation of S_1 in Southern Wallis is an important

result as it implies that deformation in the highest parts of the Alps is no longer governed by compression. It is not unusual to observe ongoing extensional deformation in convergent mountain belts. Examples of mountain belts where crustal shortening is observed along the flanks and normal faulting in the upper parts include the Andes [e.g., *Dalmayrac*, 1974; *Dorbath et al.*, 1991; *Deverchère et al.*, 1989; *Lindo*, 1993], and the Himalayas [e.g., *Molnar and Tapponier*, 1975, 1978; *Mercier et al.*, 1987; *England*, 1983]. In contrast to the aforementioned mountain belts, however, extension occurs obliquely to the strike of the belt in the central Alps and perpendicular in the western Alps.

[40] Numerous explanations for the extension have been proposed [e.g., *Molnar and Lyon-Caen*, 1988; *Avouac and Burov*, 1996; *Royden*, 1996]. The following information is relevant to establishing its cause in the Alps.

[41] 1. Both crustal thickness and topography increase from the foreland to the Alps proper. For example, across the foreland up to the Helvetic front, the European Moho lies at a depth of 28–30 km, whereas it is found at a depth of 50–58 km beneath the Insubric Line in the south (Figures 5 and 8) [*Waldhauser et al.*, 1998]. The increasing crustal thickness is accompanied by pronounced negative isostatic gravity -anomalies [*Klingelé and Kissling*, 1982]. The topography also increases from a moderate average elevation of 585 m in the foreland to an average elevation of 1880 m in the central Alps of Switzerland.

[42] 2. Deformation is ongoing: geodetic measurements show that highest rates of ongoing vertical uplift in the Alps of 1.5 mm/yr occur in the Wallis and in Graubünden [*Schlatter et al.*, 1999].

[43] In section 6.2.1. we examine the consequences of the increase in crustal thickness along our cross-strike profiles with a view to explaining the observed stress changes.

6.2.1. Gravitational Potential Energy

[44] We will investigate whether a local or "second-order" uniaxial extensional stress [*Zoback*, 1992] that might correspond to a positive gravitational potential energy stored in the thickened crust (negative density anomaly) can explain the observed extension and rotation of the horizontal stresses in the high Alps [*Artyushkov*, 1973; *Fleitout and Froidevaux*, 1982, 1983; *Molnar and Lyon-Caen*, 1988; *Coblentz at al.*, 1994]. The stress on which this local stress is superimposed will be referred to as regional or "first-order" stress, and the sum of both stresses, which is the stress actually observed, will be called the resultant stress.

[45] The orientation of the resultant stress will depend on the relative magnitudes and orientations of the regional and the local stress components which are known from our study. The strike of the crustal root is fairly well known so that the direction of the local stress, which is perpendicular to it, can be easily determined (Figure 8). However, the depth of the lithosphere is not well constrained [*Kissling*, 1993]. Available evidence suggests that beneath the central Alps the lithospheric mantle does not thicken. In the Wallis and the western Alps the lithospheric root could either dip very steeply or be absent altogether (slab break off) [*Kissling*, 1993; *Lippitsch*, 2002]. Because of this uncertainty, the influence of the mantle lid on the potential energy cannot be assessed quantitatively and the implied stress perturbation calculated. Therefore our analysis is essentially concerned only with geometric aspects of the problem.

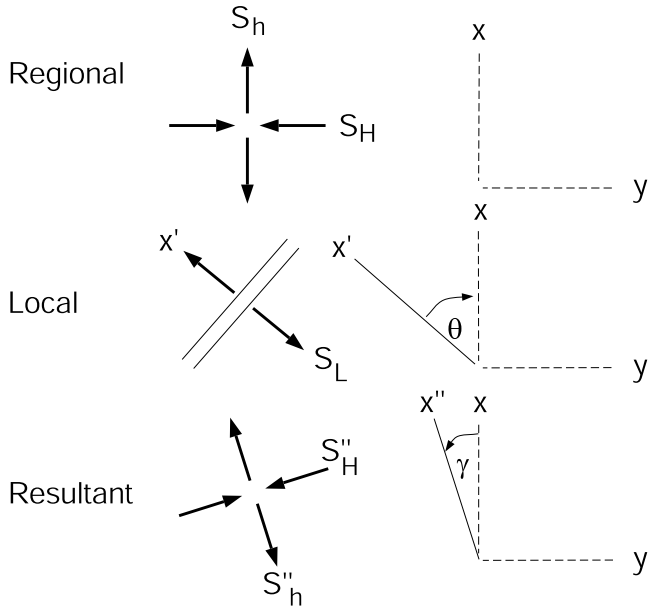

Figure 9. Illustration of the superposition of a local uniaxial stress onto a large-scale "regional" stress to yield the "resultant" stress which is the stress observed at a point. A local uniaxial stress can arise from a 2-D perturbation in Moho depth such as from a crustal root. The angles are measured anticlockwise looking downward from the regional S_h axis and follow *Zoback* [1992].

6.2.2. Decomposition of Resultant Stress Into Regional and Local Components

[46] *Sonder* [1990] and *Zoback* [1992] describe a scheme for assessing whether an observed local stress perturbation can be explained as due to the superposition of a local uniaxial stress on the regional stress. The calculation is based on simple tensor addition in the horizontal plane and is illustrated in Figure 9 [*Jaeger and Cook*, 1979; *Sonder*, 1990]. The angle γ represents the observed rotation of the perturbed S_h from the regional orientation, and the uniaxial perturbing stress is described by its magnitude, S_L and its orientation, θ, measured with respect to the regional S_h. If the regional stress magnitudes are described by S_H and S_h, then the variables are related through

$$\gamma = \frac{1}{2}\left\{\frac{\sin 2\theta}{[(S_H - S_h)/S_L] - \cos 2\theta}\right\} \qquad (1)$$

[47] Using equation (1), we can plot contours of the predicted perturbation in stress orientation, γ, as a function of the uniaxial local stress orientation, θ, for specific values of $(S_H - S_h)_{reg}/S_L$, the regional differential stress normalized by the uniaxial stress magnitude (Figure 10a). Since in the analysis both γ and θ are constrained by observations, we can obtain estimates for the normalized uniaxial local stress magnitude (in units of regional differential stress) from the contour values at the intersection of the constrained range of γ-θ values.

[48] The stress data indicate that the regional stress of western Europe, which most likely results from the ridge push in the North Atlantic and the convergence between the African and Eurasian plates, is locally disturbed in the

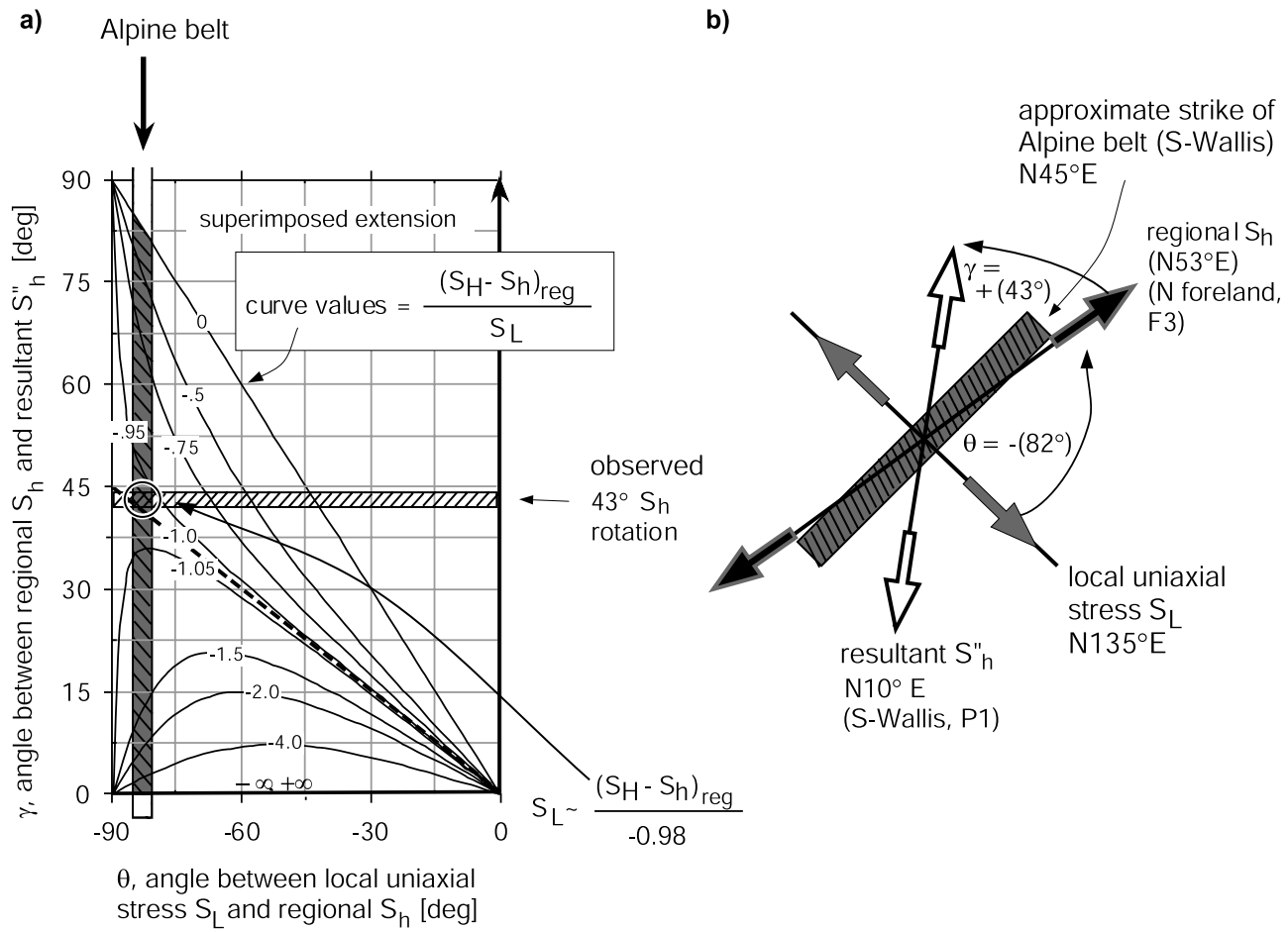

Figure 10. (a) Analysis of the rotation of the minimum horizontal stress, S_h, applied to the western central Alps (Wallis). Plot of γ, the horizontal stress rotation, as a function of θ, the angle between the local uniaxial stress and the regional S_h orientation for various values of the normalized uniaxial stress magnitude, $(S_H - S_h)/S_L$. Negative values of $(S_H - S_h)/S_L$ imply tensional stress. The vertical line indicates the constraint imposed by the observation that $\gamma = -80°$. The horizontal line denotes the constraint arising from the observation that $\theta = 45°$. The value of the $(S_H - S_h)/S_L$ contour at the intersection of the two lines of −0.95 indicates that the observed rotation of S_h across the Alpine chain in western Switzerland can be explained by the local perturbation of the large-scale regional stress by a local uniaxial tension of magnitude similar to the regional differential stress and orientation perpendicular to the strike of the Alpine belt. (b) Geometry of the stresses, stress rotation, and the strike of the crustal structure that might be responsible for the uniaxial extension stress.

vicinity of the Alps and shows a fanlike pattern along the arc (Figure 8). The horizontal stress directions in the Alps themselves do not align with this pattern but rather show a seemingly progressive, systematic rotation with respect to the stresses in the foreland (Figure 4c). Within the context of our proposed model, we will consider the rotation in stress across the Alpine chain to be the result of the superposition of a local and a regional stress. The choice of the regional stress requires some consideration owing to the tendency for observed horizontal stress directions in the foreland to rotate with position around the Alpine arc. In the analysis that follows, we consider variations in horizontal stress orientation along a profile that is normal to the local structural strike: that is, in the direction of local Moho dip (we are making here a 2-D approximation of a 3-D structure). Thus it is natural to take the regional stress as that which prevails in the foreland section of the profile in question, where the Moho depth becomes relatively stable.

6.2.3. Results of Stress Decomposition for the Central Alps (Switzerland)

[49] The crustal root in the Wallis strikes ∼N45°E (Table 6). Hence the horizontal uniaxial stress caused by the thickened crust strikes N135°E, thereby forming an angle $\theta = -82°$ with the regional S_h which is oriented N53°E (F3) (Figure 10b). This constraint on θ is shown in Figure 10a by the gray bar with black stripes. The second constraint is that the observed (i.e., resultant) stress in the southern Wallis is rotated 45° from the regional S_h, so that $\gamma = 45°$. This constraint on γ is shown in Figure 10a by the horizontal white bar with black stripes. At the intersection of the two lines in the γ-θ solution space, the contour of the stress ratio $(S_H - S_h)/S_L$ takes the value −0.98. Thus the

Table 6. Data for Evaluating Whether a Uniaxial Local Extensional Stress Perpendicular to the Crustal Root Can Be Responsible for the Observed Extension and the Rotation of the Horizontal Stresses in the Alps[a]

Region	Regional S_h	Resultant S_h	Strike of Structure Causing Extension	Azimuth of Local Uniaxial Stress	γ	θ
Wallis	N53°E (F3)	N10°E (P1)	N45°E	N135°E	43°	−82°
Graubünden	N79°E (F5)	N30°E (P2[b])	N70°E	N160°E	49°	−81°

[a]Applied to scheme on Figure 10; for details, see text. Azimuth of local uniaxial stress is perpendicular to the structure; γ is angle between regional and resultant S_h; and θ is angle between local uniaxial stress and regional S_h.
[b]Mean T axis.

normalized horizontal uniaxial stress $S_L/(S_H - S_h) = -1.02$, where the negative sign indicates that it is tensional.

[50] The data for the profile extending across eastern Switzerland into Graubünden are also listed in Table 6 and yield similar results to the Wallis profile. Here the strike of the crustal root is N70°E. If we accept the mean orientation of the T axis of N30°E as indicating the direction of the observed S_h, and take the regional S_h as oriented N79°E (F5), then we have $\gamma = 49°$ and $\theta = -81°$, values which are similar to those for the Wallis. From Figure 10a, the value of the stress ratio, $(S_H - S_h)/S_L$, at the intersection of these two values is −0.9, implying the normalized uniaxial stress, $S_L/(S_H - S_h) = -1.1$.

[51] Thus the observed rotation of S_h across the Alpine chain in western Switzerland can be explained by the local perturbation of the large-scale regional stress by a local uniaxial tension of magnitude similar to the regional differential stress and orientated perpendicular to the strike of the Alpine belt. We interpret this local stress to be a ''spreading'' stress that results from lateral density changes due to the presence of a crustal root [*Artyushkov*, 1973]. This interpretation is further supported by the observation that the rotation appears to occur gradually along the western profile, the S_3 azimuth observed in the Helvetic nappes being intermediate between those in the foreland and Penninic nappes. The superposition of this local tension with the regional stress explains why the Penninic nappes should be currently extensional. A simple consideration shows that this is the only possibility. One characteristic of the regional stress regime in the northern foreland is that S_1 and S_2 are similar in magnitude with S_3 horizontal. This means that S_1 can be horizontal or vertical, and the stress regime favors equally normal and strike-slip faulting. If we now superimpose a horizontal uniaxial tensional stress, the effect will be to reduce the net horizontal compression in all directions (except in the orthogonal direction to the uniaxial stress which will remain unchanged). Thus regardless of the relative orientation of the horizontal components of the two stresses, the superposition will always serve to reduce horizontal compression and thus move the stress state toward normal faulting.

[52] The tendency toward a slightly compressional regime in the eastern Helvetic nappes as well as in the westernmost foreland could be related to the extension in the high Alps. In a simplified consideration, the thrust-faulting component can be understood as a paired compensational deformation to the extension occurring in the adjacent higher Alps [e.g., *Molnar and Lyon-Caen*, 1988].

7. Conclusions

[53] The pervasive west European ''first-order'' stress field with S_H oriented NW-SE, which is believed to result from the ridge push in the North Atlantic and convergence between the African and Eurasian plate, is perturbed in the vicinity of the European Alps. Regional groups of fault plane solutions from earthquakes in the Swiss Alps have been inverted to determine the spatial variation of the stresses driving present-day deformation in the Swiss Alps and the northern Alpine foreland. A general feature of the stress inversion results is that the azimuth of S_3 is generally well constrained for each data set and always lies in the NE quadrant. However, the azimuth of S_3 changes systematically both along the NE structural strike of the Alpine chain and also across it. These trends are accompanied by changes in the predominant style of deformation, and are interpreted as reflecting the effects of two different ''second-order'' stress-generating mechanisms.

[54] The variation in stress along the chain involves a progressive, counterclockwise rotation of the orientation of S_h from east to west. It is most strongly defined in the foreland of our study area where it amounts to 45°–50°, and continues westward into the foreland of the western Alps [*Sue et al.*, 1999]. A rotation in the same sense is also seen in the Penninic nappes, but no such rotation can be resolved in the Helvetic nappes. The pattern of rotation in the foreland is similar to the disturbance to the stress field expected from the indentation of the Adriatic Block into the Central European Plate [*Pavoni*, 1961; *Regenauer-Lieb and Petit*, 1997]. The indentation mechanism can also explain why the NE-SW azimuth of S_3 is the most stable facet of the stress throughout the foreland and is consistent with the view that the entire central European plate gives way to the penetrating Italy/Adria Block by a NE-SW extension mechanism [*Regenauer-Lieb and Petit*, 1997]. However, buoyancy forces arising from the strongly arcuate structure of the Moho to the immediate west of our study area might also contribute.

[55] The variation in stress across the Alps is defined by a progressive, counterclockwise rotation in S_3 azimuth along two profiles in east and west Switzerland that extend from the foreland in the north across the Helvetic nappes to the Penninic nappes in the south. The net rotation along both profiles between the foreland and the Penninic nappes amounts to 40°–50°, and is accompanied by a trend toward increasing dominance of normal faulting in the south. The contrast in stress states at either end of the profiles can be explained by the superposition of a local uniaxial tension in the south whose magnitude is similar to the regional differential stress in the north and whose orientation is perpendicular to the strike of the Alpine belt. The tensile nature and orientation of this stress is consistent with the characteristics of the stress expected to result from lateral density changes due to the crustal root. This is further supported by the observation of a gradual change in the direction of S_3 as we go from the foreland to the high parts of the Alps.

[56] **Acknowledgments.** We would like to thank the Associate Editor Doug Schmitt, John Townend, Thomas Plenefisch, and an anonymous

reviewer for their very thorough reviews. We are also thankful to Klaus Regenauer-Lieb for many interesting discussions and John Gephart for providing us with his stress inversion program and for being helpful whenever problems occurred. We also appreciated that Barbara Romanowicz hosted one of the authors (U. Kastrup) for 7 months at the Seismological Laboratory at University of California, Berkeley.

References

Ahorner, L., and G. Schneider (1974), The Rhinegraben: Geologic history and neotectonic activity (in German), in *Approaches to Taphrogenesis*, edited by J. H. Illies and K. Fuchs, pp. 104–117, Schweizerbart, Stuttgart, Germany.

Ahorner, L., H. Murawski, and G. Schneider (1972), Seismotektonische Traverse von der Nordsee bis zum Apennin, *Geol. Rundsch.*, *61*(3), 915–942.

Artyushkov, E. V. (1973), Stresses in the lithosphere caused by crustal thickness inhomogeneities, *J. Geophys. Res.*, *78*(32), 7675–7708.

Avouac, J. P., and E. B. Burov (1996), Erosion as a driving mechanism of intracontinental mountain growth, *J. Geophys. Res.*, *101*(B8), 17,747–17,769.

Baer, M. (1990), The seismic station network of the Swiss Seismological Service, paper presented at Workshop on MEDNET, the Broad-Band Seismic Network for the Mediterranean, Ist. Naz. di Geofis., Rome.

Baer, M., N. Deichmann, D. Fäh, U. Kradolfer, D. Mayer-Rosa, E. Rüttener, T. Schler, S. Sellami, and P. Smit (1997), Earthquakes in Switzerland and surrounding regions during 1996, *Eclogae Geol. Helv.*, *90*(3), 557–567.

Baer, M., et al. (1999), Earthquakes in Switzerland and surrounding regions during 1998, *Eclogae Geol. Helv.*, *9*(2), 265–273.

Becker, A. (1999), In situ stress data from the Jura Mountains—New results and interpretation, *Terra Nova*, *11*, 9–15.

Becker, A. (2000), The Jura Mountains—An active foreland fold-and-thrust-belt?, *Tectonophysics*, *321*, 381–406.

Becker, A., P. Blümling, and W. H. Müller (1987), Recent stress field and neotectonics in the eastern Jura Mountains, Switzerland, *Tectonophysics*, *135*, 277–288.

Blümling, P., S. Hüsges, and M. Fejerskov (1992), Present state of stress in the Swiss Molasse Basin, *Eclogae Geol. Helv.*, *8*(3), 784–785.

Bonjer, K.-P. (1992), Seismizität als Zugang zu räumlichen und zeitlichen Anomalien der Spannungen in der Lithosphäre, in *Spannung und Spannungsumwandlung in der Lithosphäre, Berichtsband 1990–1992*, *Sonderforschungsbereich 108*, pp. 985–1031, Univ. ät Karlsruhe, Karlsruhe, Germany.

Bonjer, K.-P. (1997), Seismicity pattern and style of seismic faulting at the eastern borderfault of the southern Rhine Graben, *Tectonophysics*, *275*, 41–69.

Bonjer, K.-P., R. Gelbke, D. Gilg, D. Rouland, D. Mayer-Rosa, and B. Massinon (1984), Seismicity and dynamics of the upper Rhinegraben, *J. Geophys.*, *55*, 1–12.

Calais, E. (1999), Continuous GPS measurements across the western Alps, 1996–1998, *Geophys. J. Int.*, *138*(1), 221–230.

Carey-Gailhardis, E., and J. L. Mercier (1992), Regional state of stress, fault kinematics and adjustments of blocks in a fractured body of rock: Application to the microseismicity of the Rhine Graben, *J. Struct. Geol.*, *14*, 1007–1017.

Coblentz, D. D., R. M. Richardson, and M. Sandiford (1994), On the gravitational potential of the Earth's lithosphere, *Tectonics*, *13*(4), 929–945.

Dalmayrac, B. (1974), Un exemple de tectonique vivante: Les failles subactuelles du pied de la Cordillère Blanche (Pérou) (An example of active tectonics: The Quaternary faults at the base of the Blanca, Peru), *Cahi. ORSTOM, Sér. Géol.*, *6*, 19–27.

Deichmann, N. (1987), Focal depths of earthquakes in northern Switzerland, *Ann. Geophys., Ser. B*, *5*(4), 395–402.

Deichmann, N. (1990), Seismizität der Nordschweiz 1987–1989 und Auswertung der Erdbebenserien von Günsberg, Läufelfingen und Zeglingen, *Nagra Tech. Ber. NTB 90-46*, Nagra, Baden, Switzerland.

Deichmann, N. (1992), Structural and rheological implications of lower-crustal earthquakes below northern Switzerland, *Phys. Earth Planet. Inter.*, *69*, 270–280.

Deichmann, N., and M. Baer (1990), Earthquake focal depth below the Alps and the northern Alpine foreland of Switzerland, *The European Geotraverse: Integrative Studies*, edited by R. Freeman, P. Giese, and St. Muller, pp. 277–288, Eur. Sci. Found., Strasbourg, France.

Deichmann, N., and M. Garcia-Fernadez (1992), Rupture geometry from high-precision relative hypocenter locations of microearthquake clusters, *Geophys. J. Int.*, *110*, 501–517.

Deichmann, N., and L. Rybach (1989), Earthquakes and temperatures in the lower crust below the Alps and northern Alpine foreland of Switzerland, in *Properties and Processes of the Lower Crust*, *Geophys. Monogr. Ser.*, vol. 51, edited by R. F. Mereu, S. Mueller, and D. M. Fountain, pp. 197–213, AGU, Washington, D. C.

Deichmann, N., et al. (1998), Earthquakes in Switzerland and surrounding regions during 1997, *Eclogae Geol. Helv.*, *9*(2), 246–247.

Deichmann, N., et al. (2000a), Earthquakes in Switzerland and surrounding regions during 1999, *Eclogae Geol. Helv.*, *93*(3), 395–406.

Deichmann, N., D. Ballarin, and U. Kastrup (2000b), Seismizität der Nordschweiz, *Nagra Tech. Ber. NTB 00-05*, Nagra, Baden, Switzerland.

Delouis, B., H. Hässler, A. Cisternas, and L. Rivera (1993), Stress tensor determination in France and neighbouring regions, *Tectonophysics*, *22*, 413–438.

DeMets, C., R. G. Gordon, D. F. Argus, and S. Stein (1994), Effect of recent revisions to the geomagnetic reversal time scale on estimates of current plate motions, *Geophys. Res. Lett.*, *21*(20), 2191–2194.

Deverchère, J., C. Dorbath, and L. Dorbath (1989), Extension related to a high topography: results from a microearthquake survey in the Andes of Peru and tectonic implications, *Geophys. J. Int.*, *98*, 281–292.

Dorbath, L., C. Dorbath, E. Jimenez, and L. Rivera (1991), Seismicity and tectonic deformation in the Eastern Cordillera and the sub-Andean Zone of central Peru, *J. S. Am. Earth Sci.*, *4*(1–2), 13–24.

Dorel, J., J. Fréchet, J. Gagnepain-Beyneix, H. Haessler, M. Lachaize, R. Madariaga, and T. Modiano (1983), Focal mechanism in metropolitan France and the Lesser Antilles: French Focal Mechanism Working Group, *Ann. Geophys.*, *1*(4–5), 299–305.

England, P. (1983), Constraints on extension of continental lithosphere, *J. Geophys. Res.*, *88*(B2), 1145–1152.

Etchecopar, A., G. Vasseur, and M. Daignières (1981), An inverse problem in microtectonics for the determination of stress tensors from fault striation analysis, *J. Struct. Geol.*, *3*, 51–65.

Eva, E., and S. Solarino (1998), Variations of stress directions in the western Alpine Arc, *Geophys. J. Int.*, *132*(2), 438–448.

Eva, E., S. Solarino, C. Eva, and G. Neri (1997), Stress tensor orientation derived from fault plane solutions in the southwestern Alps, *J. Geophys. Res*, *102*(B4), 8171–8185.

Eva, E., S. Pastore, and N. Deichmann (1998), Evidence for ongoing extensional deformation in the western Swiss Alps and thrust-faulting in the southwestern Alpine foreland, *J. Geodyn.*, *26*(1), 27–43.

Evans, K., and P. Roth (1998), The state of stress in northern Switzerland inferred from earthquake seismological data and in-situ stress measurements, final report, Deep Heat Min. DHM, Steinmaur, Switzerland.

Fleitout, L., and C. Froidevaux (1982), Tectonics and topography for a lithosphere containing density heterogeneities, *Tectonics*, *1*(1), 21–56.

Fleitout, L., and C. Froidevaux (1983), Tectonic stresses in the lithosphere, *Tectonics*, *2*(3), 315–324.

Fréchet, J. (1978), Sismicité du sud-est de la France, et une nouvelle méthode de zonage sismique, Ph.D. thesis, Univ. Sci. et Méd. de Grenoble, Grenoble, France.

Fréchet, J., F. Thouvenot, L. Jenatton, P. Hoang-Trong, and M. Frogneux (1996), Le séisme du Grand-Bornand (Haute-Savoie) du 14 decembre 1994: Un coulissage dextre dans le socle subalpin, *C. R. Acad. Sci., Ser. IIa*, *323*, 517–524.

Fröhlich, A. (1989), Seismotektonik der Westschweiz unter Berücksichtigung der Bebenserie von Freiburg [1987], Romont [1988] und Boltigen [1989], Diploma thesis, Inst. of Geophys., ETH Zürich, Zürich, Switzerland.

Gebrande, H. (1976), A seismic ray-tracing method for two-dimensional inhomogenous media, in *Explosion Seismology in Central Europe: Data and Results*, edited by P. Giese, C. Prodehl, and A. Stein, pp. 162–167, Springer-Verlag, New York.

Gephart, J. W. (1990), FMSI: A FORTRAN program for inverting fault/slickenside and earthquake focal mechanism data to obtain the regional stress tensor, *Comput. Geosci.*, *16*(7), 953–989.

Gephart, J. W., and D. W. Forsyth (1984), An improved method for determining the regional stress tensor using focal mechanism data: Application to the San Fernando earthquake sequence, *J. Geophys. Res.*, *89*(B11), 9305–9320.

Greiner, G., and J. H. Illies (1977), Central Europe: Active or residual tectonic stresses, *Pure Appl. Geophys.*, *115*, 11–26.

Grünthal, G., and D. Stromeyer (1992), The Recent crustal stress field in central Europe: Trajectories and finite element modeling, *J. Geophys. Res.*, *97*(B8), 11,805–11,820.

Hardebeck, J. L., and E. Hauksson (2001), Stress orientations obtained from earthquake focal mechanisms: What are appropriate uncertainty estimates?, *Bull. Seismol. Soc. Am.*, *91*, 250–262.

Jaeger, J. C., and N. G. W. Cook (1979), *Fundamentals of Rock Mechanics*, Chapman and Hall, New York.

Jimenez, M.-J., and N. Pavoni (1983), Focal mechanisms of recent earthquakes, 1976–1982, and seismotectonics in Switzerland, paper presented at IASPEI XVIII Assembly, Hamburg, Germany.

Kastrup, U. (2002), Seismotectonics and stress field variations in Switzerland, Ph.D. thesis, ETH Zürich, Zürich, Switzerland.

Kissling, E. (1993), Deep structure of the Alps; what do we really know?, *Phys. Earth Planet. Inter.*, *79*(1–2), 87–112.

Klingéle, E., and E. Kissling (1982), Zum Konzept der isostatischen Modelle in Gebirgen am Beispiel der Schweizer Alpen, in *Schwere-Anomalien und isostatische Modelle in der Schweiz*, *Geod. Geophys. Arb. Schweiz 35*, pp. 3–36, Schweizerische Geod. Komm., Zürich, Switzerland.

Larroque, J. M., A. Etchecopar, and H. Philip (1987), Evidence for the permutation of stresses σ_1 and σ_2 in the Alpine foreland; the example of the Rhine Graben, *Tectonophysics*, *144*, 315–322.

Laubscher, H. P. (1972), Some overall aspects of Jura dynamics, *Am. J. Sci.*, *272*(4), 293–304.

Lindo, R. (1993), Sismotectonique des Andes du Pérou central: Apport des données sismologiques de haute précision (Seismotectonics of the central Peruvian Andes: Contribution of high-resolution seismologic data), Ph.D. thesis, Univ. de Strasbourg I, Strasbourg, France.

Lippitsch, R. (2002), Lithosphere and upper mantle *P*-velocity structure beneath the Alps by high-resolution teleseismic tomography, Ph.D. thesis, ETH Zürich, Zürich, Switzerland.

Marone, F. (1999), Das Magnitude 5 Beben von Vaz (Graubünden) von 1991, Seismotektonik und Auswertung der Nachbeben, Diploma thesis, Inst. of Geophys., ETH Zürich, Zürich, Switzerland.

Maurer, H. (1993), Seismotectonics and upper crustal structure in the western Swiss Alps, Ph.D. thesis, ETH Zürich, Zürich, Switzerland.

Maurer, H., and N. Deichmann (1995), Microearthquake cluster detection based on waveform similarities, with an application to the western Swiss Alps, *Geophys. J. Int.*, *123*, 588–600.

Maurer, H., M. Burkhard, N. Deichmann, and A. G. Green (1997), Active tectonism in the eestern Swiss Alps, *Terra Nova*, *9*, 91–94.

Mayer, G., P. M. Mai, T. Plenefisch, H. Echtler, E. Lüschen, V. Wehrle, B. Müller, K.-P. Bonjer, C. Prodehl, and K. Fuchs (1997), The deep crust of the southern Rhine Graben; Reflectivity and seismicity as images of dynamic processes, *Tectonophysics*, *275*, 15–40.

Mercier, J. L., R. Armijo, P. Tapponnier, E. Carey-Gailhardis, and H. T. Lin (1987), Change from late Tertiary compression to Quaternary extension in southern Tibet during the India-Asia collision, *Tectonics*, *6*(3), 275–304.

Meyer, B., R. Lacassin, J. Brulhet, and B. Mouroux (1994), The Basel 1356 earthquake: Which fault produced it?, *Terra Nova*, *6*, 54–63.

Michael, A. J. (1984), Determination of stress from slip data: Faults and folds, *J. Geophys. Res.*, *89*(B13), 11,517–11,526.

Michael, A. J. (1987), Use of focal mechanisms to determine stress: A control study, *J. Geophys. Res.*, *92*(B1), 357–368.

Molnar, P., and H. Lyon-Caen (1988), Some simple physical aspects of the support, structure, and evolution of mountain belts, in *Processes in Continental Lithospheric Deformation*, edited by S. P. Clark Jr., *Spec. Pap. Geol. Soc. Am.*, *218*, 179–207.

Molnar, P., and P. Tapponnier (1975), Cenozoic tectonics of Asia: Effects of a continental collision, *Science*, *189*(4201), 419–426.

Molnar, P., and P. Tapponnier (1978), Active tectonics of Tibet, *J. Geophys. Res.*, *83*(B11), 5361–5375.

Müller, B., M. L. Zoback, K. Fuchs, L. G. Mastin, S. Gregersen, N. Pavoni, O. Stephansson, and C. Ljunggren (1992), Regional patterns of tectonic stress in Europe, *J. Geophys. Res.*, *97*(B8), 11,783–11,803.

Müller, B., V. Wehrle, and K. Fuchs (1997), *The World Stress Map for Western Europe: The 1997 Release of the World Stress Map*, Heidelberg Acad. of Sci. and Humanities, Univ. Karlsruhe, Karlsruhe, Germany.

Pavoni, N. (1961), Faltung durch Horizontalverschiebung, *Eclogae Geol. Helv.*, *54*(2), 515–534.

Pavoni, N. (1975), Zur Seismotektonik des Westalpenbogens, *Vermessung Photogramm., Kulturtech.*, *III/IV*, 185–187.

Pavoni, N. (1977), Erdbeben im Gebiet der Schweiz (Earthquakes in Switzerland), *Eclogae Geol. Helv.*, *70*(2), 351–370.

Pavoni, N. (1980), Crustal stresses inferred from fault-plane solutions of earthquakes and neotectonic deformation in Switzerland, *Rock Mech., Suppl.*, *9*, 63–68.

Pavoni, N. (1984), Seismotektonik Nordschweiz, *NTB 84-45*, Nagra, Baden, Switzerland.

Pavoni, N. (1987), Zur Seismotektonik der Nordschweiz, *Eclogae Geol. Helv.*, *80*(2), 461–472.

Pavoni, N. (1992), Seismoactive fault systems in the basement and sedimentary cover of the Swiss Plateau and the Jura Mountains, *Eclogae Geol. Helv.*, *85*(3), 781–784.

Pavoni, N., and E. Peterschmitt (1974), Das Erdbeben von Jeurre von 21. Juni 1971 und seine Beziehungen zur Tektonik des Faltenjura (The Jeurre earthquake of June 21, 1971, and its relationship to the tectonics of the Jura Mountains), in *Approaches to Taphrogenesis*, edited by J. H. Illies and K. Fuchs, pp. 322–329, Schweizerbart, Stuttgart, Germany.

Pavoni, N., H. Maurer, P. Roth, and N. Deichmann (1997), Seismicity and seismotectonics of the Swiss Alps, in *Deep Structure of the Alps*, *Results of* NRP20, pp. 241–250, Birkhäuser, Basel, Switzerland.

Pfiffner, O. A., P. Lehner, P. Heitzmann, St. Müller, and A. Steck (1997), *Deep Structure of the Alps*, *Results of NRP20*, 380 pp., Birkhäuser, Basel, Switzerland.

Plenefisch, T., and K.-P. Bonjer (1997), The stress field in the Rhine Graben area inferred from earthquake focal mechanisms and estimation of frictional parameters, *Tectonophysics*, *275*, 71–97.

Regenauer-Lieb, K., and J. P. Petit (1997), Cutting of the European continental lithosphere; plasticity theory applied to the present Alpine collision, *J. Geophys. Res.*, *10*(B4), 7731–7746.

Roth, P. (1986), Untersuchungen über den gegenwärtigen Deformations- und Spannungszustand der Erdkruste im Gebiet der Schweiz mit Hilfe von Nahbeben-Stationsdiagrammen, Diploma thesis, Inst. of Geophys., ETH Zürich, Zürich, Switzerland.

Roth, P. (1990), Aktuelle Seismizität und Seismotektonik in den östlichen Schweizer Alpen (Recent seismicity and seismotectonics in the eastern Swiss Alps), Ph.D. Thesis, ETH Zürich, Zürich, Switzerland.

Roth, P., N. Pavoni, and N. Deichmann (1992), Seismotectonics of the eastern Swiss Alps and evidence for precipitation induced variations of seismic activity, *Tectonophysics*, *207*, 183–197.

Royden, L. (1996), Coupling and decoupling of crust and mantle in convergent orogens; Implications for strain partitioning in the crust, *J. Geophys. Res.*, *101*(B8), 17,679–17,705.

Sambeth, U., and N. Pavoni (1988), A seismotectonic investigation in the Geneva Basin, southern Jura Mountains, *Eclogea Geol. Helv.*, *8*(2), 433–440.

Schlatter, A., H.-G. Kahle, and E. Gubler (1999), Investigations of recent uplift rates in Switzerland using repeated first order levellings, in *Report on the Geodetic Activities in the Years 1995 to 1999*, p. 62, Swiss Geod. Comm., Zürich, Switzerland.

Schmid, S. M., and E. Kissling (2000), The arc of the western Alps in the light of geophysical data on deep crustal structure, *Tectonics*, *19*(1), 62–85.

Schmid, S. M., O. A. Pfiffner, N. Froitzheim, G. Schoenborn, and E. Kissling (1996), Geophysical-geological transect and tectonic evolution of the Swiss-Italian Alps, *Tectonics*, *15*(5), 1036–1064.

Schmid, S. M., O. A. Pfiffner, and G. Schreurs (1997), Rifting and collision in the Penninic zone of Eastern Switzerland, in *Deep Structure of the Alps*, *Results of NRP20*, pp. 160–185, Birkhäuser, Basel, Switzerland.

Smit, P. (1989), Seismotektonische und aeromagnetische Untersuchungen in der Region Ramsen (Kanton Schaffhausen), Diploma thesis, Inst. of Geophys., ETH Zürich, Zürich, Switzerland.

Sonder, L. J. (1990), Effects of density contrasts on the orientation of stresses in the lithosphere: Relation to principal stress directions in the Transverse Ranges, California, *Tectonics*, *9*(4), 761–771.

Sue, C., F. Thouvenot, J. Fréchet, and P. Tricart (1999), Widespread extension in the core of the western Alps revealed by earthquake analysis, *J. Geophys. Res.*, *104*(B11), 25,611–25,622.

Thouvenot, F. (1981), Modélisation bidimensionelle de la croûte terrestre en vitesse et atténuation des ondes sismiques (Implications géodynamiques pour les Alpes Occidentales), Ph.D. thesis, Univ. Grenoble, Grenoble, France.

Thouvenot, F., et al. (1998), The M_L = 5.3 Epagny (French Alps) earthquake of 15 July 1996: A long awaited event on the Vuache fault, *Geophys. J. Int.*, *135*, 876–892.

Waldhauser, F., E. Kissling, J. Ansorge, and St. Müller (1998), Three-dimensional interface modelling with two-dimensional seismic data: The Alpine crust-mantle boundary, *Geophys. J. Int.*, *135*(1), 264–278.

Wyss, M., B. Liang, W. R. Tanigawa, and K. Wu (1992), Comparision of orientation of stress and strain tensors based on fault plane solutions in Kaoiki, Hawai, *J. Geophys. Res.*, *97*(B4), 4769–4790.

Zoback, M. L. (1992), First- and second-order patterns of stress in the lithosphere: The World Stress Map Project, *J. Geophys. Res.*, *97*(B8), 11,703–11,711.

N. Deichmann, D. Giardini, and U. Kastrup, Institute of Geophysics, ETH-Hönggerberg, CH-8093 Zürich, Switzerland. (nico@seismo.ifg.ethz.ch; giardini@seismo.ifg.ethz.ch; ulrike@kastrup.net)

K. F. Evans, Geology Institute, ETH-Hönggerberg, CH-8093 Zürich, Switzerland. (keith.evans@erdw.ethz.ch)

A. J. Michael and M. L. Zoback, Western Region Earthquake Hazard Team, U.S. Geological Survey, 345 Middlefield Road, MS 977, Menlo Park, CA 94025, USA. (zoback@usgs.gov; michael@usgs.gov)